THE ASTRONOMICAL JOURNAL, 115:2285–2305, 1998 June

THE DEMOGRAPHY OF MASSIVE DARK OBJECTS IN GALAXY CENTERS

JOHN MAGORRIAN,[1] SCOTT TREMAINE,[1,2] DOUGLAS RICHSTONE,[3] RALF BENDER,[4] GARY BOWER,[5] ALAN DRESSLER,[6] S. M. FABER,[7] KARL GEBHARDT,[3] RICHARD GREEN,[5] CARL GRILLMAIR,[8] JOHN KORMENDY,[9] AND TOD LAUER[5]

Received 1997 August 7; revised 1998 March 2

ABSTRACT

We construct dynamical models for a sample of 36 nearby galaxies with *Hubble Space Telescope* (*HST*) photometry and ground-based kinematics. The models assume that each galaxy is axisymmetric, with a two-integral distribution function, arbitrary inclination angle, a position-independent stellar mass-to-light ratio Υ, and a central massive dark object (MDO) of arbitrary mass $M_\bullet$. They provide acceptable fits to 32 of the galaxies for some value of $M_\bullet$ and Υ; the four galaxies that cannot be fitted have kinematically decoupled cores. The mass-to-light ratios inferred for the 32 well-fitted galaxies are consistent with the fundamental-plane correlation $\Upsilon \propto L^{0.2}$, where L is galaxy luminosity. In all but six galaxies the models require at the 95% confidence level an MDO of mass $M_\bullet \sim 0.006 M_{\rm bulge} \equiv 0.006 \Upsilon L$. Five of the six galaxies consistent with $M_\bullet = 0$ are also consistent with this correlation. The other (NGC 7332) has a much stronger upper limit on $M_\bullet$. We predict the second-moment profiles that should be observed at *HST* resolution for the 32 galaxies that our models describe well.

We consider various parameterizations for the probability distribution describing the correlation of the masses of these MDOs with other galaxy properties. One of the best models can be summarized thus: a fraction $f \simeq 0.97$ of early-type galaxies have MDOs, whose masses are well described by a Gaussian distribution in $\log (M_\bullet/M_{\rm bulge})$ of mean -2.28 and standard deviation ~ 0.51. There is also marginal evidence that $M_\bullet$ is distributed differently for "core" and "power law" galaxies, with core galaxies having a somewhat steeper dependence on $M_{\rm bulge}$.

Key words: dark matter — galaxies: nuclei

1. INTRODUCTION

The evidence that massive dark objects (MDOs) are present in the centers of nearby galaxies is reviewed by Kormendy & Richstone (1995, hereafter KR95). Further evidence that postdates this review is described by Bender, Kormendy, & Dehnen (1996), Kormendy et al. (1997), and van der Marel et al. (1997b). The MDOs are probably black holes, since star clusters of the required mass and size are difficult to construct and maintain, and since black hole quasar remnants are expected to be common in galaxy centers; however, this identification is not important for the purposes of this paper. Following Kormendy (1993a), KR95 suggest that at least 20% of nearby kinematically hot galaxies (ellipticals and spiral bulges) have MDOs and point out that the observed MDO masses exhibit the correlation $M_\bullet \simeq 0.003 M_{\rm bulge}$, where $M_{\rm bulge}$ is the mass of the hot stellar component of the galaxy (throughout this paper we use the word "bulge" to refer to the hot stellar component of a galaxy, whether elliptical or spiral). For a "bulge" with constant mass-to-light ratio Υ and luminosity L, $M_{\rm bulge} \equiv \Upsilon L$.

The machinery for modeling the kinematics of bulges to determine whether MDOs are present has increased steadily in sophistication over the past two decades. The earliest models (e.g., Sargent et al. 1978) fitted only the line-of-sight velocity dispersions of spherical galaxies and assumed that the stellar distribution function was isotropic. Modern programs (e.g., Rix et al. 1997; Gebhardt et al. 1997) fit the entire line-of-sight velocity distribution for arbitrary axisymmetric galaxy models. While the most general and accurate possible models, and the highest resolution spectroscopic observations, were needed to establish the presence of the first few MDOs, we have learned with experience that estimates of the MDO mass based on cruder models and observations are usually fairly accurate. An example is the MDO in M87: Sargent et al. (1978) estimated the mass to be $\sim 5 \times 10^9\, M_\odot$ from spherical, isotropic models, very close to the $3 \times 10^9\, M_\odot$ determined by Harms et al. (1994) from *Hubble Space Telescope* (*HST*) spectra of a ring of ionized gas at 20 pc from the center.

This experience suggests that it is worthwhile to estimate MDO masses using relatively simple models applied to a large sample of galaxies. We cannot yet insist on *HST* spectroscopy for our sample, since this is still available only for a few galaxies; on the other hand, *HST* photometry is available for over 60 galactic bulges. In this paper, we examine a sample of 36 bulges for which both *HST* photometry and reasonable-quality, ground-based, long-slit spectroscopy are available. We look for evidence of MDOs among these by fitting two-integral axisymmetric dynamical models to

[1] Canadian Institute for Theoretical Astrophysics, University of Toronto, 60 St. George Street, Toronto, ON M5S 3H8, Canada.
[2] Canadian Institute for Advanced Research Cosmology and Gravity Program.
[3] Department of Astronomy, University of Michigan, 830 Dennison Building, Ann Arbor, MI 48109.
[4] Universitäts-Sternwarte, Scheinerstrasse 1, D-81679 München, Germany.
[5] Kitt Peak National Observatory, National Optical Astronomy Observatories, P.O. Box 26732, Tucson, AZ 85726.
[6] Observatories of the Carnegie Institution of Washington, 813 Santa Barbara Street, Pasadena, CA 91101.
[7] UCO/Lick Observatory, Board of Studies in Astronomy and Astrophysics, University of California, Santa Cruz, CA 95064.
[8] Jet Propulsion Laboratory, Mail Stop 183-900, 4800 Oak Grove Drive, Pasadena, CA 91109.
[9] Institute for Astronomy, University of Hawaii, 2680 Woodlawn Drive, Honolulu, HI 96822.

the data for each galaxy. These are not the most general types of models, but they are quick to compute and will guide us toward galaxies to which we should apply more precise (and expensive) observations and models. Our results also provide a first look at the statistical distribution of MDOs as a function of galaxy luminosity and other parameters. They do *not* establish unambiguously that an MDO is present in any individual galaxy.

The paper is organized as follows: The next section gives a brief outline of the data we use. This is followed by a detailed description of our modeling procedure and the assumptions that go into it. Section 4 presents results for individual galaxies. What these tell us about the MDO mass distribution is tackled in § 5. Finally, § 6 sums up.

2. DATA

Our sample consists of all reasonably dust-free galaxy bulges with *HST* photometry and ground-based velocity dispersion and rotation velocity profiles. The sample contains 36 galaxies, listed in Table 1 along with details about the sources of the observations that we use. Appendix A contains comments about some of the galaxies. Most of the objects were observed prior to the first *HST* servicing mission with the Planetary Camera (0″.043 pixel^{-1}) through filter F555W (roughly Johnson *V*). The sample includes galaxies observed in a number of *HST* programs (Lauer et al. 1992b, 1992a; Grillmair et al. 1994; Jaffe et al. 1994; Forbes, Franx, & Illingworth 1995; Lauer et al. 1995); the reduction procedures are described by Lauer et al. (1995), Byun et al. (1996), and Faber et al. (1997). Some of the galaxies show evidence of nuclear activity. For each of these, the table lists a radius $R_{\rm min}$ inside which nonstellar radiation probably makes a significant contribution to the observed light.

The *HST* data extend only to about 10″ from the center. For most of the galaxies, we take published ground-based photometry and join it smoothly to the *HST* data to obtain a global photometric profile. For the remaining galaxies, we assume that the outer parts are well described by an $R^{1/4}$ profile with the same flattening as the outermost *HST* isophote. We take the effective radius of the $R^{1/4}$ profile from the literature, if available; otherwise we estimate it by fitting to the *HST* photometry.

Table 1 also lists the sources for our kinematic data. We restrict ourselves to reasonable-quality CCD-based spectroscopy. Because the kinematics predicted by our models at any point depends on the details of the photometry at larger radii, we do not use kinematic data beyond about two-thirds of the maximum radius for which photometry is available. Whenever there are many sources for a given slit position of a galaxy, we generally choose those with the best seeing. If an estimate for the seeing is unavailable, we simply assume an FWHM of 2″; we find that the MDO masses yielded by our models are fairly insensitive to the precise value used, as long as it lies between 1″ and 3″.

The observations yield line-of-sight rotational speeds and velocity dispersions, convolved with seeing and averaged over spatial "bins" determined by the slit width and pixel size. We combine the measured rotational speed v_j and the velocity dispersion σ_j in each bin j to obtain an estimate of the second-order moment $\mu_j^2 = v_j^2 + \sigma_j^2$, which is the input used by our models. Strictly speaking, the v_j and σ_j quoted by observers do not individually have any direct connection with the moments of the line-of-sight velocity profiles, since they are usually obtained by fitting Gaussians to the velocity profiles (van der Marel & Franx 1993). However, tests with flattened isotropic toy galaxies (Dehnen & Gerhard 1994; Magorrian & Binney 1994) show that there is typically an almost constant difference of about 10% between the combination $v_j^2 + \sigma_j^2$ and the true second-order moments, with the sign of the difference changing from the major to the minor axis. Figure 1 shows a typical example. Since these differences are almost constant, they do not affect the ratio of the MDO mass to the galaxy mass fitted by our models. They could, however, have a small effect on the fitted mass-to-light ratios.

Deriving the observational uncertainty $\Delta\mu_j$ is a vexing problem because analysis methods used by different observers yield a range of error estimates Δv_j and $\Delta\sigma_j$, which

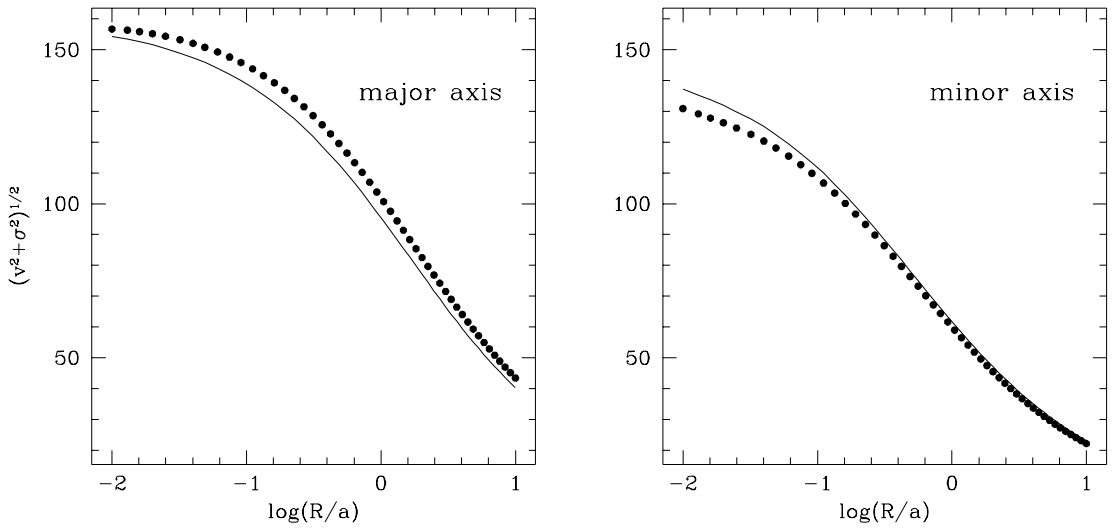

FIG. 1.—Major- and minor-axis projected second-moment profiles for a flattened (axis ratio $q = 0.6$) isotropic (rotating) Jaffe (1983) model viewed edge-on. The curves show the (square root of the) classical second-order moments. The points plot the approximation $(v^2 + \sigma^2)^{1/2}$, where v and σ are the parameters of the best-fitting Gaussians to the line-of-sight velocity profiles.

TABLE 1

GALAXY SAMPLE

Galaxy (1)	Type (2)	M_V (3)	R_{min} (arcsec) (4)	Outer Photometry (5)	Slit Position (6)	Seeing (arcsec) (7)	Maximum Radius (arcsec) (8)	Number of Bins (9)	Kinematic Source (10)
M31	S∩	−19.82	...	1	Major (bulge)	0.6	8.9	34	9
					Major (bulge)	0.75	8.2	18	10
					Minor (bulge)	1.2	8.3	17	10
					Major (nucleus)	1.16	10	19	10
					Minor (nucleus)	0.75	8.3	17	10
M32	E\	−16.60	...	2	Major	0.52	4	16	11
					Major	0.75	7.5	13	10
					Minor	0.83	11.3	9	10
					45° diagonal	0.83	12	18	10
NGC 821	E\	−20.64	...	3	Major	2.0	11.3	8	12
					Major	2.0	27.5	24	13
					Minor	2.0	17.5	16	13
NGC 1399	E∩	−21.71	...	4	Major	2.0	37.3	12	4
					Minor	2.0	38.5	12	4
NGC 1600	E∩	−22.70	...	3	Major	2.0	24.9	23	14
					Major	2.0	27	22	13
					Minor	2.0	18.4	18	14
					Minor	2.0	18.5	16	13
NGC 1700	E\	−21.65	...	4	Major	2.0	23.8	8	12
					Major	2.0	20	11	4
					Minor	2.0	20.5	7	12
					Minor	2.0	19.6	11	4
NGC 2300	E∩	−21.82	...	3	Major	2.0	15.2	8	12
					Major	2.0	21.5	18	13
					Minor	2.0	29.6	8	12
					Minor	2.0	20	19	13
NGC 2778	E\	−20.33	...	5	Major	2.0	5.5	7	15
					Major	2.0	11.5	10	13
					Minor	2.0	3.9	9	14
					Minor	2.0	10	10	13
NGC 2832	E∩	−22.95	...	5	Major	2.0	25.6	13	15
NGC 3115	S0\	−20.75	...	3	Major	0.57	43.8	56	16
					Major	2.0	21.2	56	12
					Major	1.0	30.7	25	17
					Major	1.0	28.4	20	17
					Major	1.0	24.7	23	17
					Minor	1.0	6.7	10	17
NGC 3377	E\	−19.70	...	6	Major	0.59	22.6	30	18
					Major	0.47	1.5	18	18
					Minor	2.0	28.5	26	13
NGC 3379	E∩	−20.55	...	5	Major	1.5	11.5	9	19
					18° diagonal	1.5	11.5	8	19
					28° diagonal	1.5	11.6	8	19
					72° diagonal	1.5	11.5	8	19
NGC 3608	E∩	−20.84	...	3	Major	2.0	37.3	21	14
					Major	2.0	24.5	20	13
					Minor	2.0	25.9	17	14
					Minor	2.0	24	19	13
NGC 4168	E∩	−21.76	...	3	Major	2.0	30.6	11	12
					Major	1.5	7.8	6	20
NGC 4278	E∩	−21.16	0.1	$R_{eff} = 32''$ (l)	Major	2.0	31	36	13
					Minor	2.0	30	30	13
NGC 4291	E∩	−20.85	...	3	Major	2.0	28	21	14
					Major	2.0	19.5	13	12
					Minor	2.0	24.1	17	14
					Minor	2.0	16.5	12	12
NGC 4365	E∩	−22.06	...	$R_{eff} = 57''$ (l)	Major	2.0	7.5	7	12
					Minor	2.0	6.3	6	12
NGC 4467	E\	−17.04	...	$R_{eff} = 10''$ (f)	Major	1.5	7.5	6	20
NGC 4472	E∩	−22.57	...	5	Major	2.0	23.9	18	12
					Minor	2.0	27.9	14	12
NGC 4473	E∩	−20.80	...	3	Major	2.0	20.4	11	12
NGC 4486	E∩	−22.38	...	5	Major	0.79	5.8	27	21
NGC 4486B	E∩	−17.57	...	$R_{eff} = 1''$ (f)	Major	0.66	5.5	15	22
					Major	0.52	1.1	11	22
					Minor	2.0	7.4	5	20
NGC 4494	E\	−21.14	...	3	Major	2.0	32.3	14	12
					Minor	2.0	36.8	20	14
NGC 4552	E∩	−21.05	0.1	$R_{eff} = 30''$ (l)	Major	3.0	24.9	8	12
					Major	3.0	34.5	42	13
					Minor	3.0	33.5	36	13

TABLE 1—*Continued*

Galaxy (1)	Type (2)	M_V (3)	R_{min} (arcsec) (4)	Outer Photometry (5)	Slit Position (6)	Seeing (arcsec) (7)	Maximum Radius (arcsec) (8)	Number of Bins (9)	Kinematic Source (10)
NGC 4564.....	E\	−19.94	...	3	Major	2.0	33.2	16	12
NGC 4589.....	E∩	−21.69	...	$R_{eff} = 30''$ (f)	Major	2.0	8.1	5	12
NGC 4594.....	S0\	−21.78	0.1	7	Major	0.93	4.7	19	7
					Major	0.93	4.9	11	7
					Major	0.93	5	15	10
					Major	0.93	4.2	7	10
					Minor	0.93	8.2	10	7
NGC 4621.....	E\	−21.27	...	3	Major	2.0	33.6	19	12
					Minor	2.0	27.1	16	12
NGC 4636.....	E∩	−21.67	...	3	Major	3.0	33.5	15	12
NGC 4649.....	E∩	−22.14	...	3	Major	2.0	24.2	13	12
					Major	2.0	37.5	35	13
					Minor	2.0	27.7	16	12
					Minor	2.0	34.5	52	13
NGC 4660.....	E\	−18.86	...	6	Major	2.0	8.1	8	12
					Minor	2.0	5.5	6	12
NGC 4874.....	E∩	−23.54	...	5	26° diagonal	2.0	22.5	10	15
NGC 4889.....	E∩	−23.36	...	3	Major	2.0	21.3	11	15
NGC 6166.....	E∩	−23.47	0.2	$R_{eff} = 56''$ (l)	Major	2.0	12.9	13	15
					Minor	2.0	5.5	9	15
NGC 7332.....	S0\	−19.91	...	8	Major	2.0	31.3	33	8
					Major	2.0	41.7	41	8
					Minor	2.0	9.9	16	8
					45° diagonal	2.0	19.6	33	8
					Minor + 6″	2.0	12.5	10	8
					Major + 6″	2.0	14.1	14	8
NGC 7768.....	E∩	−22.93	0.4	$R_{eff} = 30''$ (l)	Major	2.0	5.5	10	15
					Minor	2.0	4.8	6	15

NOTES.—Col. (2) gives the galaxy type: "S" = spiral bulge, "S0" = lenticular, "E" = elliptical; "∩" = cored, "\" = power law (Lauer et al. 1995). The absolute V magnitudes of the bulge or other hot component in col. (3) are taken from Faber et al. 1997 and assume $H_0 = 80$ km s^{-1} Mpc^{-1}. R_{min} in col. (4) is the radius inside which we believe the galaxy light may be contaminated by nonstellar radiation. Col. (5) gives the source of the outer photometry used (if available), otherwise it gives the effective radius R_{eff} used for the outward extrapolation. Values of R_{eff} obtained from the literature are followed by an "(l)," while an "(f)" follows those obtained by fitting to the *HST* photometry. Cols. (6)–(10) list the kinematic data used. For each exposure along each slit position, cols. (6) and (7) give the position and FWHM of the seeing, respectively. The maximum radius and the number of bins used by our models are given in cols. (8) and (9). Finally, col. (10) gives the source of the kinematic data.

REFERENCES.—(1) Kent 1987; (2) Lauer et al. 1992a; (3) Bender, Döbereiner, & Möllenhoff 1987; (4) Franx, Illingworth, & Heckman 1989; (5) Peletier et al. 1990; (6) Scorza & Bender 1995; (7) Kormendy 1988; (8) Fisher, Illingworth, & Franx 1994; (9) Kormendy & Bender 1998; (10) van der Marel et al. 1994; (11) Bender et al. 1996; (12) Bender et al. 1994; (13) González 1993; (14) Jedrzejewski & Schechter 1989; (15) Fisher et al. 1995; (16) Kormendy et al. 1996b; (17) Kormendy & Richstone 1992; (18) Kormendy et al. 1998; (19) Gebhardt et al. 1997; (20) Bender & Nieto 1990; (21) van der Marel 1994; (22) Kormendy et al. 1997.

usually do not take systematic effects, such as template mismatch, into account. We have tried the following three methods of dealing with this problem:

1. Simply take all quoted errors at face value.
2. Replace Δv_j with max (Δv_j, 5 km s^{-1}), and similarly for $\Delta\sigma_j$.
3. Scale the errors for each exposure along each slit position such that they are consistent with axisymmetry. More precisely, suppose there are n measurements σ_j^+ along one side of a galaxy, with corresponding measurements σ_j^- along the other side. We scale the $\Delta\sigma_j$ by a constant factor such that

$$\chi_\sigma^2 \equiv \sum_{j=1}^{n} \frac{(\sigma_j^+ - \sigma_j^-)^2}{(\Delta\sigma_j^+)^2 + (\Delta\sigma_j^-)^2} = n\,, \qquad (1)$$

and similarly for the Δv_j (Davies & Birkinshaw 1988).

Note that the last method implicitly assumes that the errors are Gaussian. This is almost certainly wrong, but it is the best we can do given the heterogeneous nature of our data. Given the "improved" observational errors, the error in μ_j is $\Delta\mu_j = [v_j^2(\Delta v_j)^2 + \sigma_j^2(\Delta\sigma_j)^2]^{1/2}/\mu_j$ to first order. We use method 3 above whenever possible, but the results of our models are usually not significantly affected by which procedure we employ.

3. MODELING PROCEDURE

We assume that each galaxy is axisymmetric, with some unknown inclination angle i, and work in cylindrical coordinates (R, ϕ, z), where the z-axis is the symmetry axis of the galaxy. A lower bound on i comes from requiring that all isophotes have an intrinsic axis ratio no less than 0.3 (i.e., no flatter than E7). Each galaxy can have a central MDO of arbitrary mass, but otherwise the mass-to-light ratio Υ is assumed to be independent of position. The distribution function of the stars is assumed to be a function only of two integrals of motion, the energy and the z-component of angular momentum. The advantage of these assumptions is that the (even part of the) kinematics follows uniquely from the three-dimensional luminosity distribution $\nu(R, z)$ (see, e.g., Lynden-Bell 1962; Dejonghe 1986). The disadvantage is that there is no reason why real galaxies should obey our assumptions. In particular, our two-integral models have intrinsic second-order moments $\sigma_R \equiv \sigma_z$ and $\overline{v_R v_z} \equiv 0$ and are simply the flattened generalization of spherical isotropic models. In Appendix B, we address the objections that have

been raised against the two-integral assumption and also consider alternative, radially anisotropic models.

We use the modeling procedure introduced by Binney, Davies, & Illingworth (1990) to predict the kinematics of each galaxy for any assumed inclination angle i and MDO mass $M_\bullet$. It predicts the second-order moments, convolved with seeing and averaged over the same $j = 1, \ldots, n$ spatial bins used in the observations. The procedure is as follows:

1. Use a scheme based on maximum penalized likelihood to find a smooth luminosity density $\nu(R, z)$ that projects to an acceptable fit to the observed surface brightness (Magorrian 1998). The density ν is not uniquely determined by the surface brightness unless the galaxy is edge-on (Rybicki 1987). Romanowsky & Kochanek (1997) demonstrate that even for quite high inclinations there can be a large range in ν consistent with a given surface brightness; however, they find that the effect of this uncertainty on the projected second-order moments is smaller than typical observational errors. We have carried out some experiments that confirm that the allowable MDO masses are not strongly affected by the indeterminacy in $\nu(R, z)$.
2. Calculate the gravitational potential and forces using an assumed stellar mass-to-light ratio Υ_0 and MDO mass $M_\bullet$.
3. Use the Jeans equations to calculate the second-order moments $\overline{\nu v_\phi^2}$ and $\overline{\nu v_R^2} = \overline{\nu v_z^2}$.
4. Project the luminosity-weighted zeroth- and second-order moments of the line-of-sight velocity along the line of sight, convolve with seeing, and average over the same spatial bins used in the observations.

Dividing the binned, seeing-convolved second-order moment by the corresponding zeroth-order one yields the model's predictions $\hat{\mu}_j^2(i, \Upsilon_0, M_\bullet)$ in each bin. These predictions scale trivially with the mass-to-light ratio Υ through

$$\hat{\mu}_j^2(i, \Upsilon, M_\bullet) = \frac{\Upsilon}{\Upsilon_0}\, \hat{\mu}_j^2(i, \Upsilon_0, \Upsilon_0\, M_\bullet/\Upsilon)\,. \tag{2}$$

3.1. *Estimation of $M_\bullet$ and Υ*

We assume that the measurement errors in the μ_j are Gaussian and uncorrelated. Then the likelihood of the photometric and kinematic data D given the model parameters $(i, \Upsilon, M_\bullet)$ is

$$\Pr\,(D \,|\, i, \Upsilon, M_\bullet) \propto \exp\,(-\tfrac{1}{2}\chi^2)\,, \tag{3}$$

where

$$\chi^2(i, \Upsilon, M_\bullet) \equiv \sum_{j=1}^{n} \left(\frac{\mu_j - \hat{\mu}_j}{\Delta\mu_j}\right)^2 . \tag{4}$$

We obtain the best-fitting values $M_\bullet$ and Υ and their confidence intervals as follows: By Bayes's theorem, the posterior distribution of i, Υ, and $M_\bullet$ given the data D is

$$\Pr\,(i, \Upsilon, M_\bullet \,|\, D) \propto \Pr\,(D \,|\, i, \Upsilon, M_\bullet)\, \Pr\,(i \,|\, q')\, \Pr\,(\Upsilon)\, \Pr\,(M_\bullet)\,, \tag{5}$$

where we have made the assumption that i, Υ, and $M_\bullet$ are a priori independent. Our priors $\Pr\,(M_\bullet)$ and $\Pr\,(\Upsilon)$ are flat in $M_\bullet$ and $\log \Upsilon$, respectively.[10] We make the reasonable assumption that the prior for i depends only on the observed axis ratio q' of the galaxy. Then $\Pr\,(i \,|\, q')$ can be related to $N(q)dq$, the probability that a randomly chosen galaxy will have an intrinsic axis ratio lying between q and $q + dq$, by a further application of Bayes's theorem:

$$\begin{aligned}\Pr\,(i \,|\, q') &= \frac{\Pr\,(i)\, \Pr\,(q' \,|\, i)}{\Pr\,(q')} \\ &\propto \Pr\,(i) \int \Pr\,(q' \,|\, i, q) N(q) dq \\ &\propto \frac{1}{\sqrt{q'^2 - \cos^2 i}}\, N\left[\frac{(q'^2 - \cos^2 i)^{1/2}}{\sin i}\right], \end{aligned} \tag{6}$$

where we have made the natural assumption that $\Pr\,(i) = \sin i$ and have used the relation $\Pr\,(q' \,|\, i, q) \propto q'\delta(q^2 \sin^2 i + \cos^2 i - q'^2)$. We approximate the $N(q)$ obtained by Tremblay & Merritt (1995) by a Gaussian centered on $q = 0.7$ with standard deviation 0.1. Our results are only very weakly dependent on this form.

We are interested mainly in $M_\bullet$ and Υ, not in i. Marginalizing the latter, we obtain the joint posterior distribution of Υ and $M_\bullet$ as

$$\Pr\,(\Upsilon, M_\bullet \,|\, D) = \Pr\,(D \,|\, \Upsilon, M_\bullet)\, \Pr\,(\Upsilon)\, \Pr\,(M_\bullet)\,, \tag{7}$$

where

$$\Pr\,(D \,|\, \Upsilon, M_\bullet) \equiv \int \Pr\,(D \,|\, i, \Upsilon, M_\bullet)\, \Pr\,(i \,|\, q') di\,. \tag{8}$$

The posterior distributions $\Pr\,(M_\bullet \,|\, D)$ and $\Pr\,(\Upsilon \,|\, D)$ follow by marginalizing equation (7) again.

4. RESULTS FOR INDIVIDUAL GALAXIES

We have made models of each of our 36 galaxies for a range of $M_\bullet \geq 0$, Υ, and i. The models do not provide adequate descriptions of the kinematics of four of the galaxies (NGC 1700, 4365, 4494, and 4589). For these four, Figure 2 shows how the χ^2 of equation (4) varies with MDO mass $M_\bullet$ and inclination angle i. Figure 3 plots the kinematics of the models with the best-fitting values of $M_\bullet$ against the observations. All four galaxies are known to have kinematically distinct cores (see, e.g., Forbes et al. 1996), so it is perhaps not surprising that our axisymmetric models do not work for them. We omit these four in the demographic analysis in the next section. For comparison, only two (NGC 3608 and NGC 4278) of the 32 galaxies that our models do fit are known to have kinematically distinct cores.

The models describe the kinematics of all of the remaining 32 galaxies reasonably well for some value of $M_\bullet$. Figure 4 shows the posterior distribution $\Pr\,(\Upsilon, M_\bullet \,|\, D)$ in each case. Figure 5 shows the kinematics of the best-fitting models along each slit position fitted. Six of these galaxies have independent determinations of the mass of a central MDO. The comparison between the best-fit masses as determined here and the mass estimates in the literature for these six is presented in Figure 6. For all but one galaxy, we obtain MDO masses that are in good agreement with those from earlier work. This gives us some degree of confidence in the assumptions that go into our models. The one exception is NGC 3115, for which Kormendy et al. (1996b) infer an MDO mass of about $2 \times 10^9\ M_\odot$, some 5 times larger than our present mass estimate.

[10] In some respects, a flat prior in $\log M_\bullet$ would be more natural; however, we wanted our program to return zero or even negative values of $\log M_\bullet$ if these were indicated by the data.

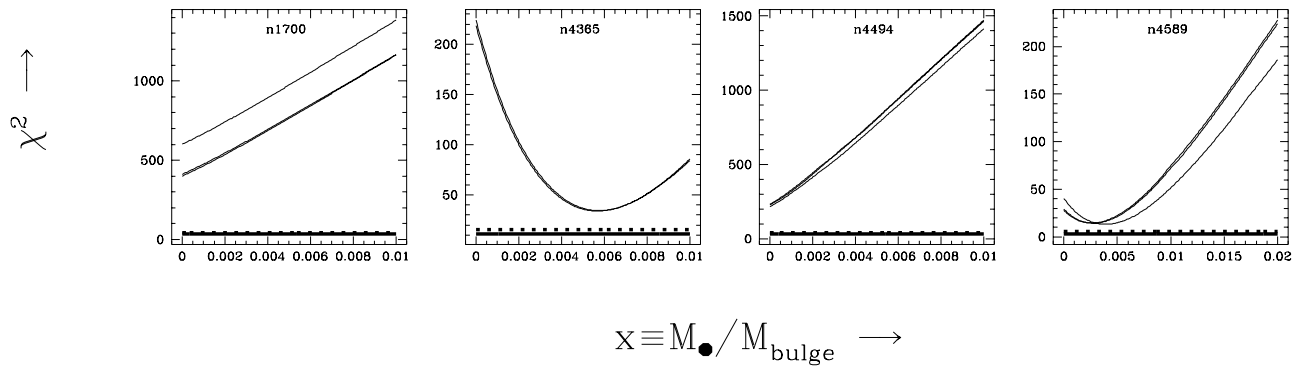

FIG. 2.—Plots of χ^2 vs. $M_\bullet/M_{\rm bulge}$ for the four galaxies that our models do not describe well. The different curves in each plot correspond to different assumed inclinations. A reasonable fit would have $\chi^2 \approx N_{\rm dof} \pm (2N_{\rm dof})^{1/2}$, where the number of degrees of freedom, $N_{\rm dof}$, is related to n, the number of kinematic bins used in the fit, by $N_{\rm dof} = n - 2$. The heavy solid and dashed lines show $\chi^2 = N_{\rm dof}$ and $\chi^2 = N_{\rm dof} + (2N_{\rm dof})^{1/2}$, respectively. The parameters ($M_\bullet$, Υ) of the best-fit model to each case are as follows: $M_\bullet = 0$, $\Upsilon_V = 5.7\ \Upsilon_\odot$ (NGC 1700); $M_\bullet = 2.3 \times 10^9\ M_\odot$, $\Upsilon_V = 7.1\ \Upsilon_\odot$ (NGC 4365); $M_\bullet = 0$, $\Upsilon_V = 4.0\ \Upsilon_\odot$ (NGC 4494); and $M_\bullet = 9.7 \times 10^8\ M_\odot$, $\Upsilon_V = 6.1\ \Upsilon_\odot$ (NGC 4589).

Our models imply that only three of the 32 galaxies (NGC 2778, 4467, and 7332) are consistent (at the 68% confidence level) with $M_\bullet = 0$. However, Figures 4 and 5 show that the available data for each of these three are also consistent with a reasonably large value of $M_\bullet$. NGC 7332 has the strongest upper limit on $M_\bullet$. In fact, the central dip in its dispersion profile is suggestive of either a mass-to-light ratio that decreases close to the center, or else strong tangential anisotropy. Kormendy (1993b) has suggested that its formation history may be different from the other galaxies in the sample. We do not, however, omit it in the analysis below. There are a further three galaxies (NGC 4168, 4473, and 4636) consistent with $M_\bullet = 0$ at the 95% confidence level.

All the other galaxies require $M_\bullet > 0$, which is easily understood as follows: The line-of-sight velocity dispersion of one of our two-integral models with central density profile $\nu \sim r^{-\alpha}$ and no MDO varies with projected radius R as

$$\sigma_p^2 \sim \begin{cases} R^{2-\alpha}, & \text{if } \frac{3}{2} < \alpha < 3, \\ R^{\alpha-1}, & \text{if } 1 < \alpha < \frac{3}{2}, \\ \text{const}, & \text{if } 0 < \alpha < 1 \end{cases} \tag{9}$$

(Dehnen 1993; Tremaine et al. 1994). Most of our cored galaxies have $\alpha < 1$ while most of our power-law galaxies have α between 1.5 and 2 (Gebhardt et al. 1996). Thus the projected dispersion of a galaxy without an MDO is con-

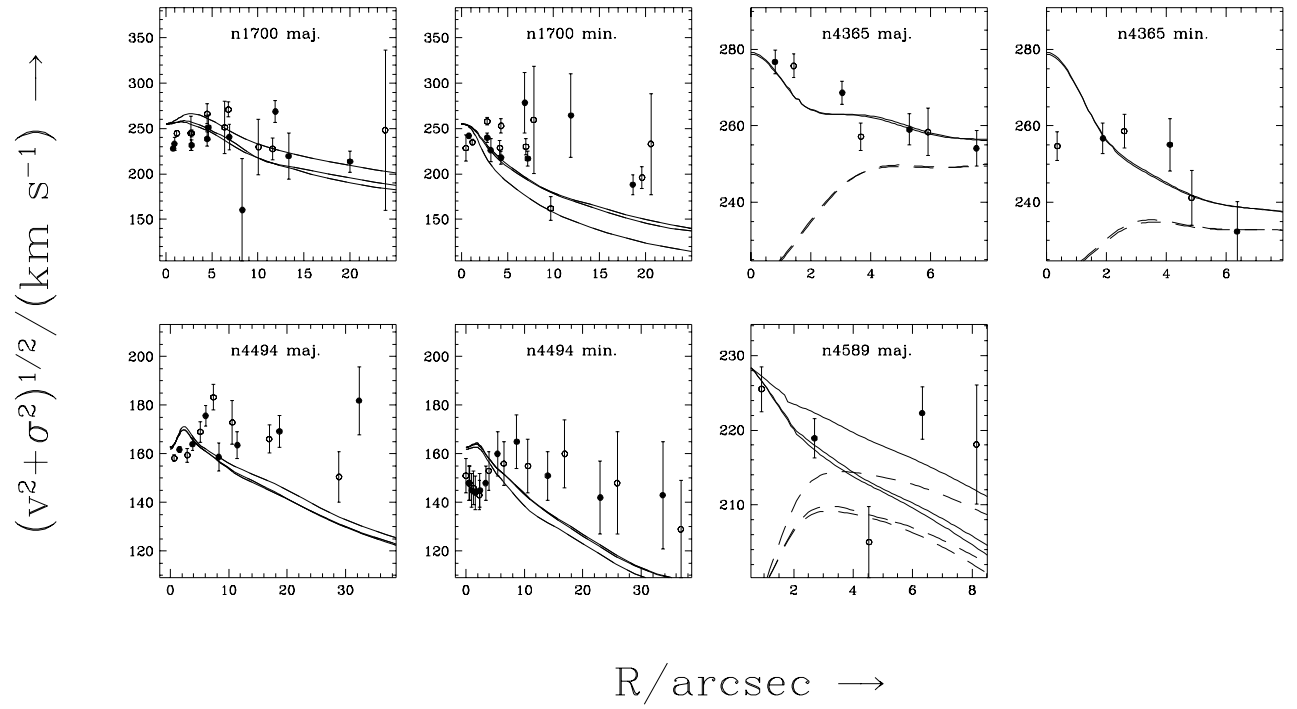

FIG. 3.—Kinematic profiles of the best-fitting models along each slit position used for the galaxies in Fig. 2. The plots show $(v^2 + \sigma^2)^{1/2}$ (in units of km s^{-1}) vs. distance from the center of the galaxy (in arcseconds). The observed kinematics is plotted as circles, open or filled depending on which side of the galaxy the observation was made. The solid curves show the model predictions (convolved with the same seeing as the best ground-based observations) for the best-fitting values of $M_\bullet$ and Υ for each galaxy. The results for each assumed inclination angle are plotted as separate curves. For comparison, the dashed curves plot the model predictions with the same value of Υ as above but $M_\bullet = 0$.

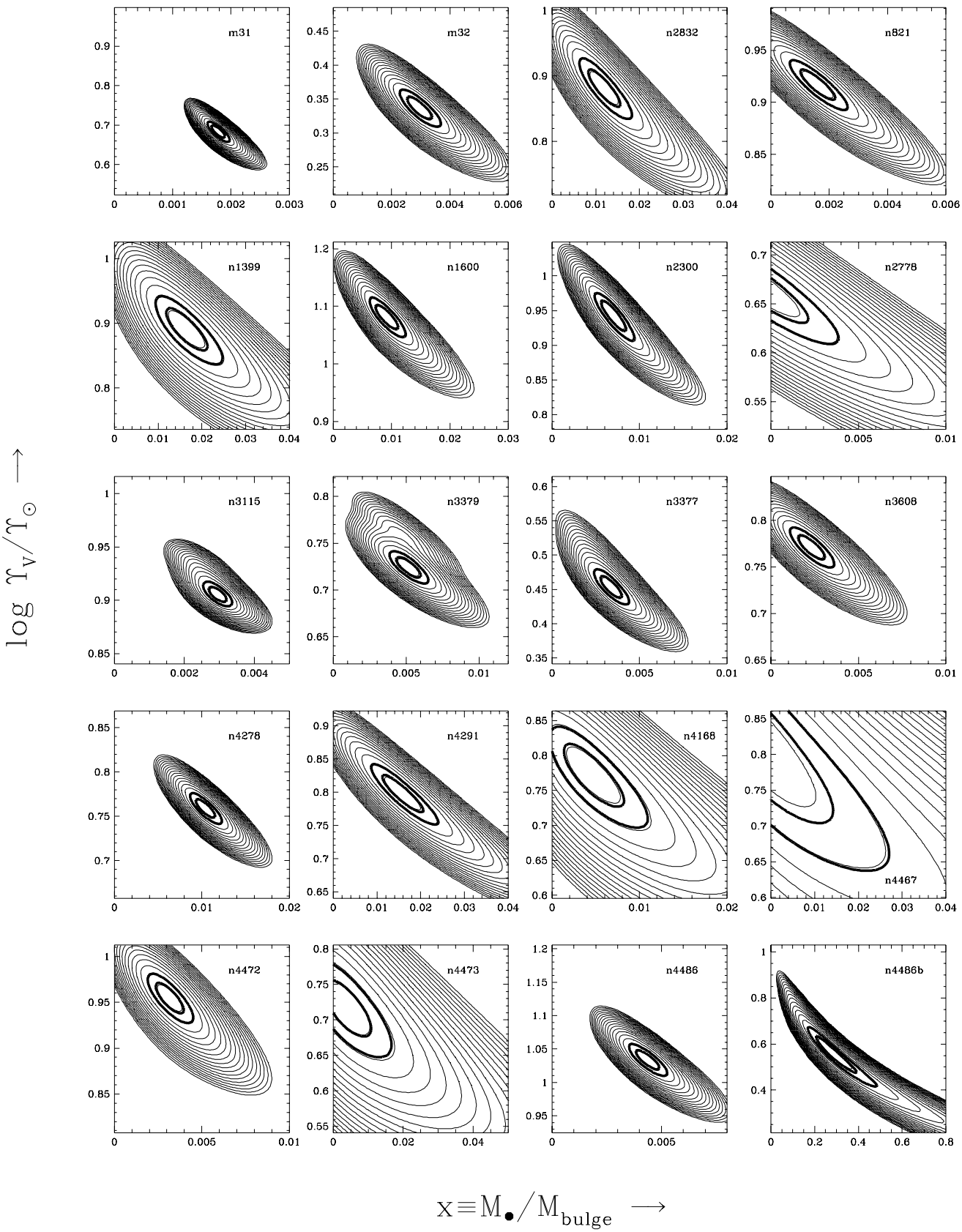

FIG. 4.—Posterior distributions Pr (Υ, $M_\bullet \mid D$) for all 32 galaxies that our models describe well. Successive light contours indicate a factor of 10 change in Pr (Υ, $M_\bullet \mid D$). The heavy contours enclose the 68% and 95% confidence regions on Υ and $M_\bullet$.

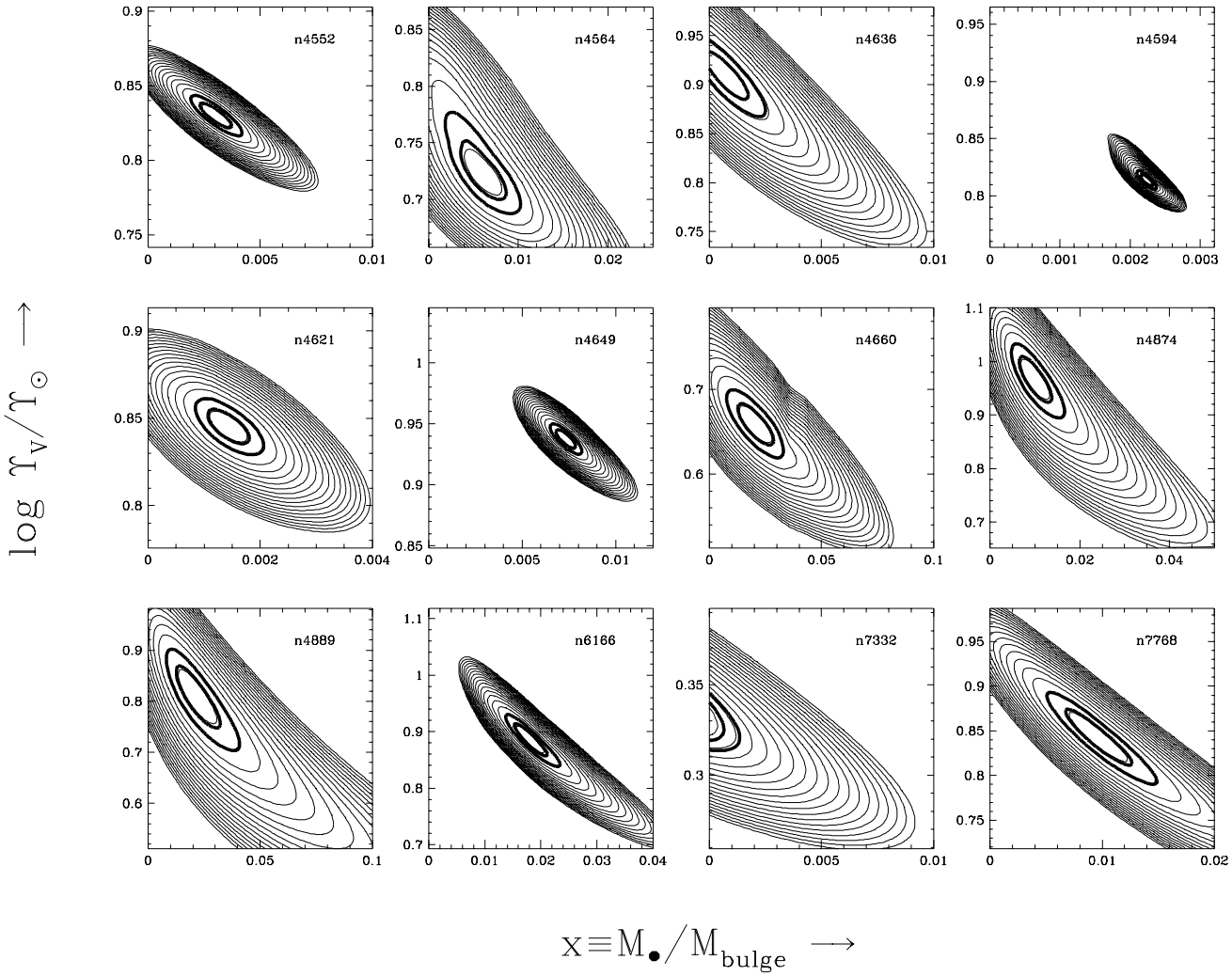

FIG. 4.—*Continued*

stant (for cored galaxies) or falls to zero (for most power-law galaxies) at the center. The MDO is required by the models in order to reproduce the central rise that is observed in the second-moment profile of most galaxies.

Five of the 32 galaxies show evidence of nuclear activity or strong dust obscuration. For these we make two types of models: one under the naive assumption that all the observed light near the galaxy center comes from stars, the other using only the photometry beyond a radius R_{min}, where R_{min} is given in Table 1. We find that the MDO masses predicted by the two types of models generally agree quite well. This is unsurprising given the relatively poor spatial resolution of the kinematic data. In what follows, we use only the MDO masses obtained by omitting photometry within R_{min}.

The kinematics predicted by our best-fit models for each galaxy when viewed with 0″.1 FWHM seeing through a 0″.2 square aperture (such as might be expected from *HST*) is plotted in Figure 7. There are four galaxies in our sample for which these *HST* measurements are already available: M32 (van der Marel, de Zeeuw, & Rix 1997a; we use only their "0.25-PAIR" observations here), NGC 3115 (Kormendy et al. 1996b), NGC 3379 (Gebhardt et al. 1997), and NGC 4594 (Kormendy et al. 1996a). These measurements are shown on the plots for these galaxies in the figure, demonstrating that our models, which use only ground-based spectroscopy, predict the kinematics observed by *HST* reasonably well. The predictions for NGC 3115 are systematically slightly too low, which suggests that our $M_\bullet \simeq 4 \times 10^8\ M_\odot$ is an underestimate (Kormendy et al. 1996b). For NGC 4594, the observed central dispersion is significantly lower than the model prediction, but this galaxy shows signs of nuclear activity, so the disagreement in this one point is not surprising. Similarly, our innermost predictions for the other four galaxies (NGC 4278, 4552, 6166, and 7768) with $R_{min} \neq 0$ in Table 1 should be viewed with some suspicion.

Table 2 lists the 68% confidence bounds that our models place on $M_\bullet$ and Υ for the 32 galaxies. The correlations between Υ and L and between $M_\bullet$ and M_{bulge} are plotted in Figure 8. Ignoring the error bars on Υ, the formal best-fit straight line to ($\log L$, $\log \Upsilon$) is

$$\log (\Upsilon_{fit}/\Upsilon_\odot) = -1.11 \pm 0.33 + (0.18 \pm 0.03) \log (L/L_\odot) \quad (10)$$

with an rms deviation between $\log \Upsilon_{fit}$ and $\log \Upsilon$ of 0.12. Our crude fit is broadly consistent with the fundamental-plane correlation $\Upsilon \propto L^{0.2}$ predicted using the virial theorem (e.g., Faber et al. 1987; Bender, Burstein, & Faber

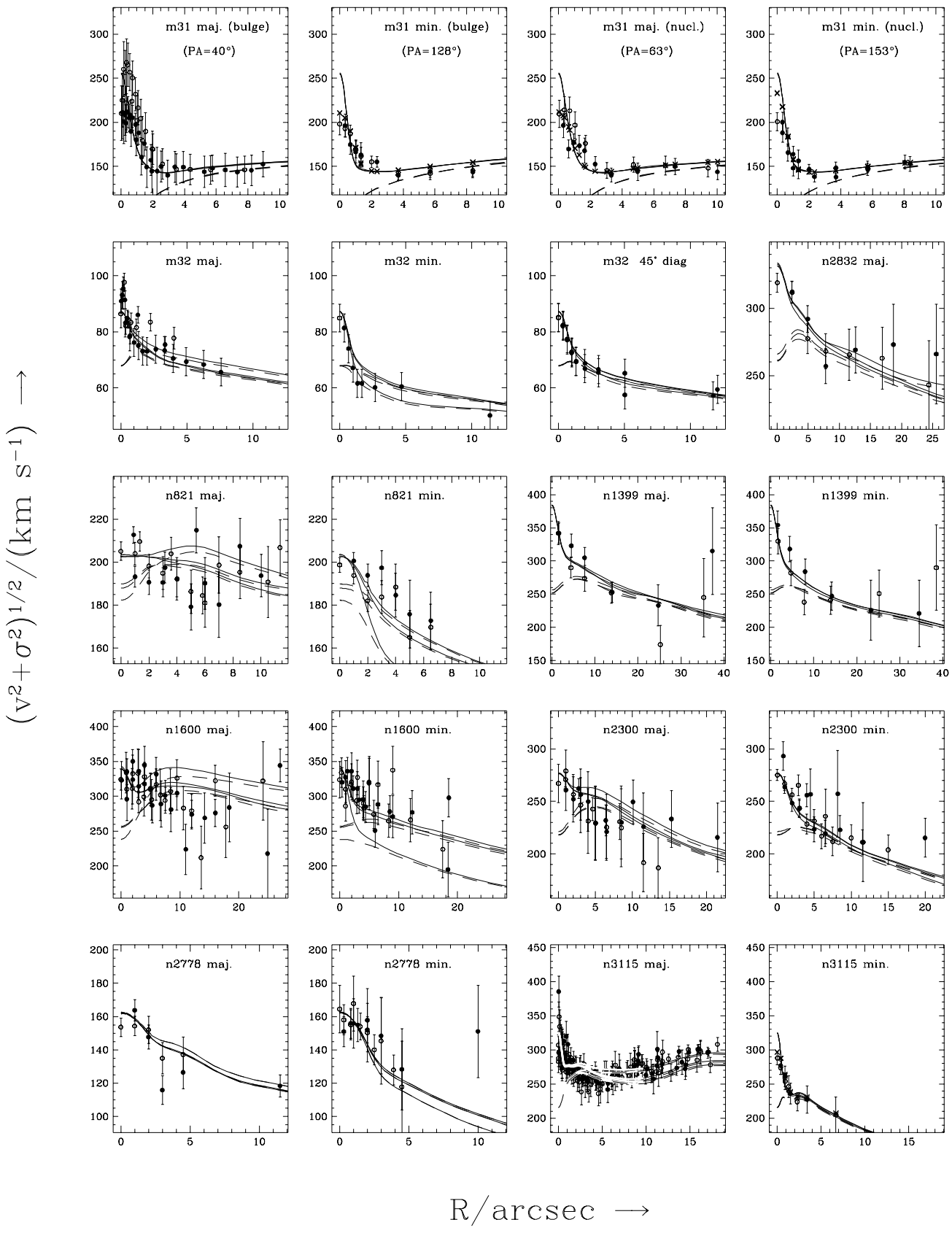

FIG. 5.—Same as Fig. 3, but for the galaxies that our models describe well. We also plot crosses to show the *spatially binned*, seeing-convolved model predictions for those cases in which this quantity differs significantly from the unbinned model predictions (described by the curves).

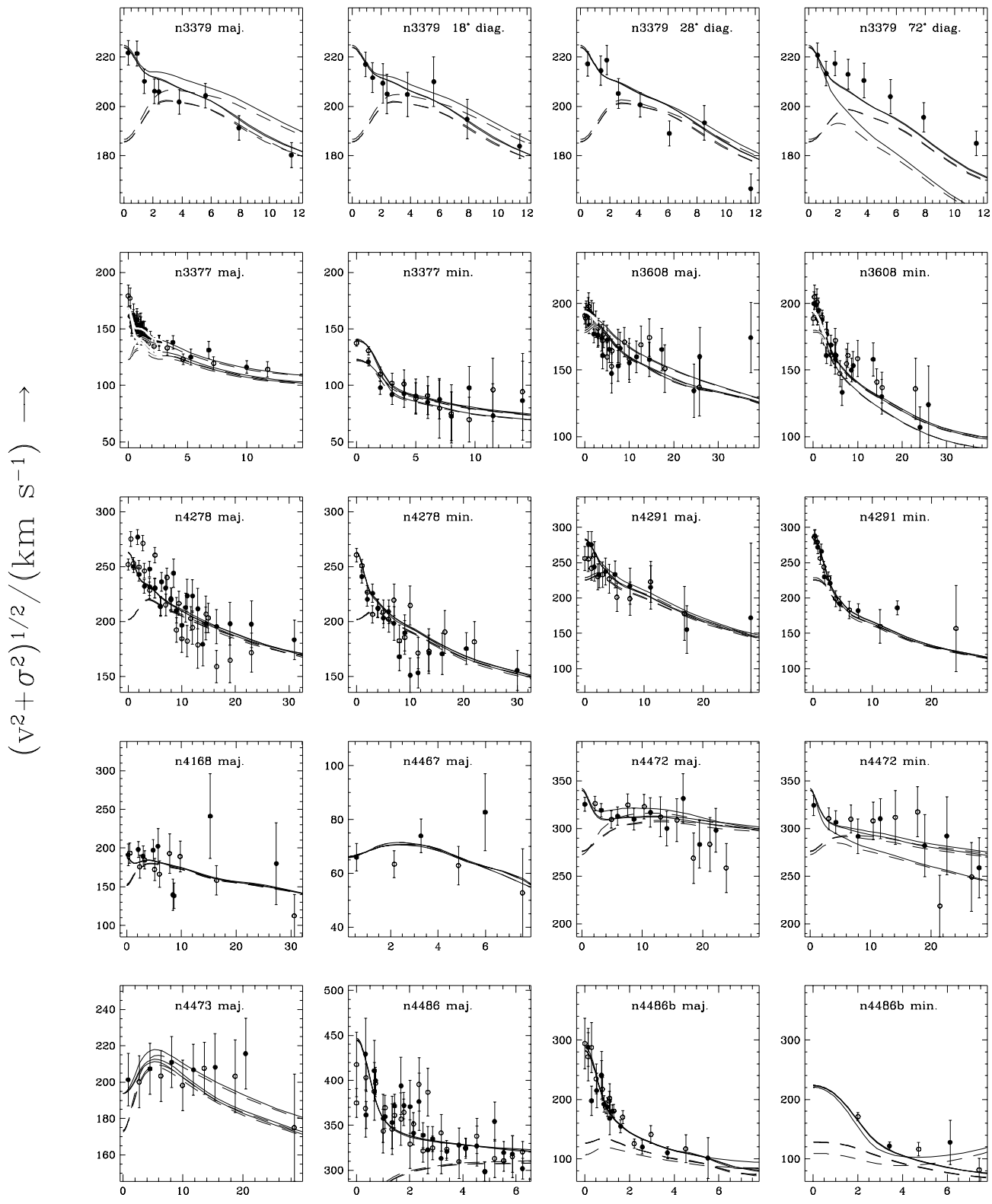

FIG. 5.—*Continued*

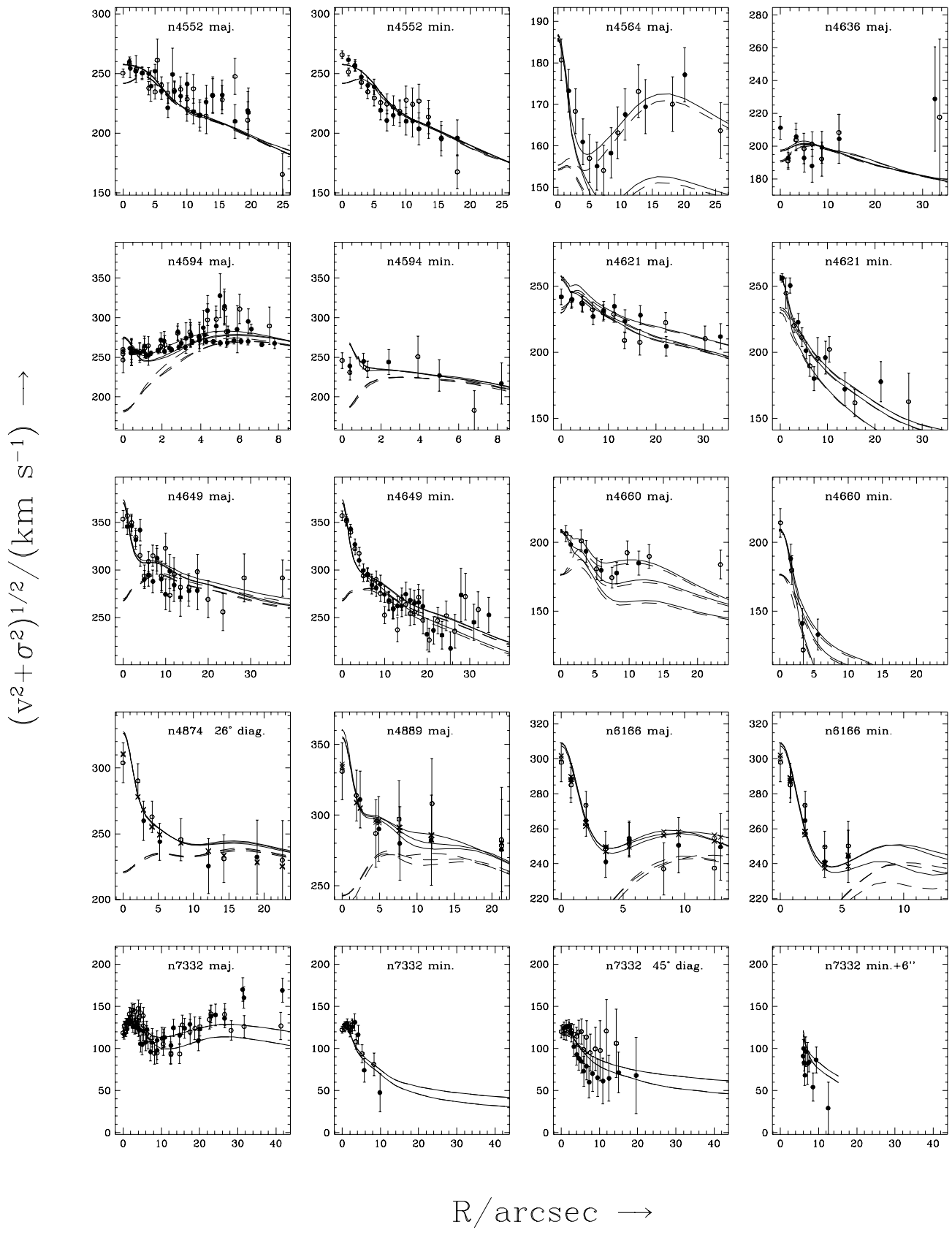

FIG. 5.—*Continued*

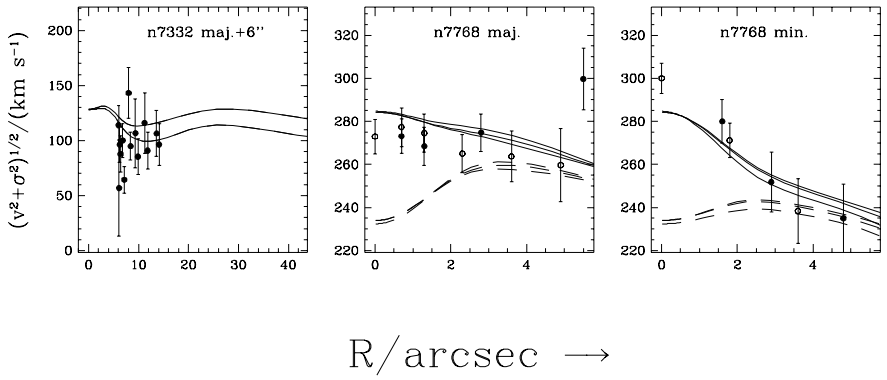

FIG. 5.—*Continued*

1992). Similarly, the correlation between $M_\bullet$ and $M_{\rm bulge}$ for those galaxies with $M_\bullet > 0$ can be described by

$$\log (M_{\bullet,\rm fit}/M_\odot) = -1.79 \pm 1.35 + (0.96 \pm 0.12) \log (M_{\rm bulge}/M_\odot)\ , \quad (11)$$

with an rms ($\log M_{\bullet,\rm fit} - \log M_\bullet$) of 0.49, although there are hints of systematic differences between power-law and core galaxies. This result is consistent with the proportionality $M_\bullet \propto M_{\rm bulge}$ that was first pointed out by Kormendy (1993a) and KR95. This apparent correlation is the subject of the next section.

Finally, we check whether there is any correlation between the residuals $x_i \equiv \log M_{\bullet,i} - \log M_{\bullet,{\rm fit},i}$ and $y_i \equiv \log \Upsilon_i - \log \Upsilon_{{\rm fit},i}$. One might expect a negative correlation if our models were fitting spuriously high MDO masses for some galaxies, thus depressing the fitted value of Υ. Figure 9 shows that there is no such correlation. The correlation coefficient $r_{xy} = 0.014$, which is not significant.

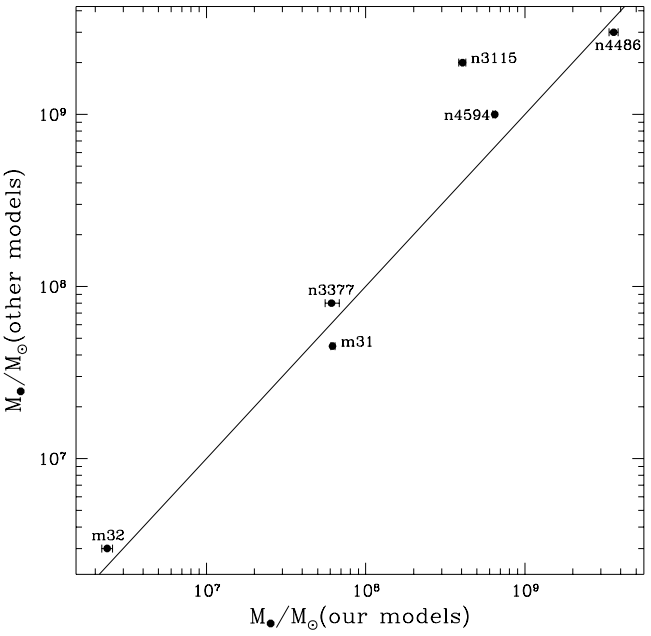

FIG. 6.—Correlation between the MDO masses predicted by our models and those predicted by other methods. The error bars give the 68% confidence limits on $M_\bullet$. Sources for the other models are as follows: M31, Richstone, Bower, & Dressler (1990); M32, van der Marel et al. (1997b); NGC 3377, Richstone et al. (1998); NGC 3115, Kormendy et al. (1996b); NGC 4594, Kormendy et al. (1996a); NGC 4486, Harms et al. (1994).

5. MDO MASS DISTRIBUTION

What do these new results tell us about the distribution of MDOs among galaxies? Let us assume initially that the MDO mass distribution of our sample depends only on $x \equiv M_\bullet/M_{\rm bulge}$ and is characterized by some other parameters ω; that is, that there is some function $\Pr(x\,|\,\omega)dx$ that is the probability that a galaxy has an MDO with mass in the range $[x, x + dx]$.

We experiment with several parameterizations P for $\Pr(x\,|\,\omega)$, as shown in Table 3. In each case, one of the parameters, f, is the fraction of galaxies with $M_\bullet > 0$, so that $\Pr(x\,|\,\omega)$ is of the form

$$\Pr(x\,|\,\omega, P) = (1-f)\delta(x) + f \Pr{}_+(x\,|\,\omega, P)\ , \quad (12)$$

where $\Pr_+(x\,|\,\omega, P)$ describes the distribution of MDOs with $M_\bullet > 0$. The $N(\omega)$ in $\Pr_+(x\,|\,\omega, P)$ is a normalizing factor chosen such that

$$\int_0^\infty \Pr{}_+(x\,|\,\omega, P)dx = 1\ . \quad (13)$$

The parameterizations $P_{\rm PL2}$ and $P_{\rm LG}$ assume that there is a genuine ridge line in $\Pr(x)$ at $x = x_0$, whereas the other three also test whether KR95's apparent ridge at $x \simeq 0.005$ is just the upper envelope of some ridgeless $\Pr(x)$.

For each parameterization $P = P_{\rm PL1}, P_{\rm PL2}, P_{\rm S}, P_{\rm G}, P_{\rm LG}$, we first seek the most likely set of parameters ω given our data D. By Bayes's theorem, the posterior distribution of ω and mass-to-light ratios $\boldsymbol{\Upsilon} \equiv (\Upsilon_1, \ldots, \Upsilon_N)$ of the 32 galaxies is

$$\Pr(\omega\boldsymbol{\Upsilon}\,|\,D, P) \propto \Pr(\omega\,|\,P) \Pr(\boldsymbol{\Upsilon}) \Pr(D\,|\,\omega\boldsymbol{\Upsilon}, P)$$
$$\propto \Pr(\omega\,|\,P) \Pr(\boldsymbol{\Upsilon}) \int \Pr(D\,|\,\boldsymbol{\Upsilon}\boldsymbol{x}) \Pr(\boldsymbol{x}\,|\,\omega, P)d\boldsymbol{x}\ , \quad (14)$$

where $\Pr(D\,|\,\boldsymbol{\Upsilon}\boldsymbol{x})$ is a product of factors of the form of equation (8). The prior $\Pr(\omega\,|\,P)$ is assumed flat in the parameters ω given in Table 3. We are interested only in the parameters ω, not in $\boldsymbol{\Upsilon}$. Marginalizing the latter yields

$$\Pr(\omega\,|\,D, P) = \int \Pr(\omega\boldsymbol{\Upsilon}\,|\,D, P)d\boldsymbol{\Upsilon}$$
$$\propto \Pr(\omega\,|\,P) \int \Pr(D\,|\,\boldsymbol{x}) \Pr(\boldsymbol{x}\,|\,\omega, P)d\boldsymbol{x}$$
$$\propto \Pr(\omega\,|\,P) \prod_{j=1}^{N} \int \Pr(D_j\,|\,x_j) \Pr(x_j\,|\,\omega, P)dx_j\ , \quad (15)$$

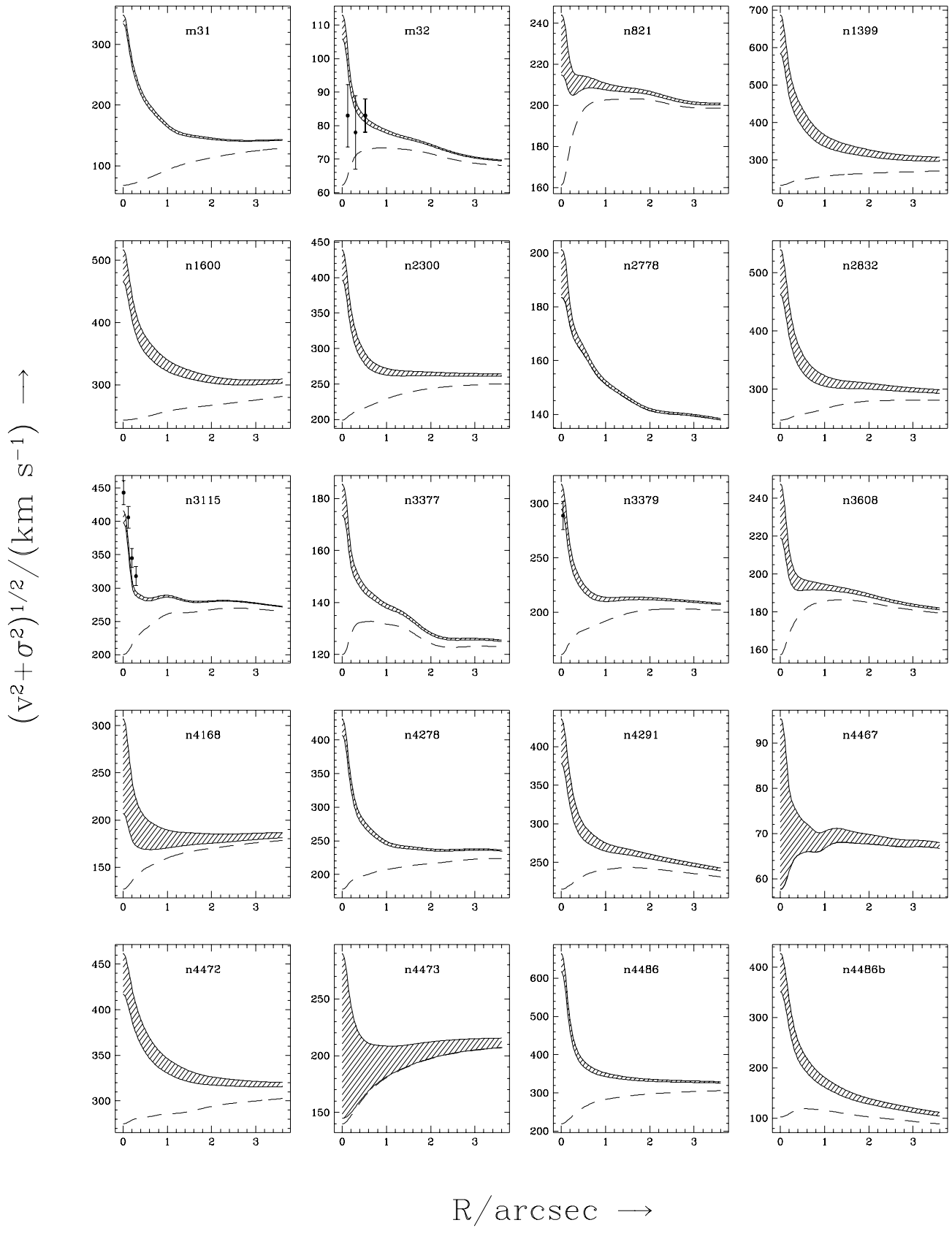

FIG. 7.—Major-axis kinematics predicted by our models when viewed with 0.″1 FWHM seeing through a 0.″2 square aperture, similar to *HST* observing conditions. The hatched areas in each panel show the predictions for edge-on models with Υ and $M_\bullet$ within the 68% confidence limits given in Table 2. For comparison, the dashed curves show predictions for $M_\bullet = 0$. The corresponding *HST* measurements are available for M32 (van der Marel, de Zeeuw, & Rix 1997a), NGC 3115 (Kormendy et al. 1996b), NGC 3379 (Gebhardt et al. 1997), and NGC 4594 (Kormendy et al. 1996a) and are also plotted in the relevant panels. The models' predictions for the inner regions of NGC 4278, 4552, 4594, 6166, and 7768 are suspect because of the presence of nuclear activity or central dust obscuration in these galaxies.

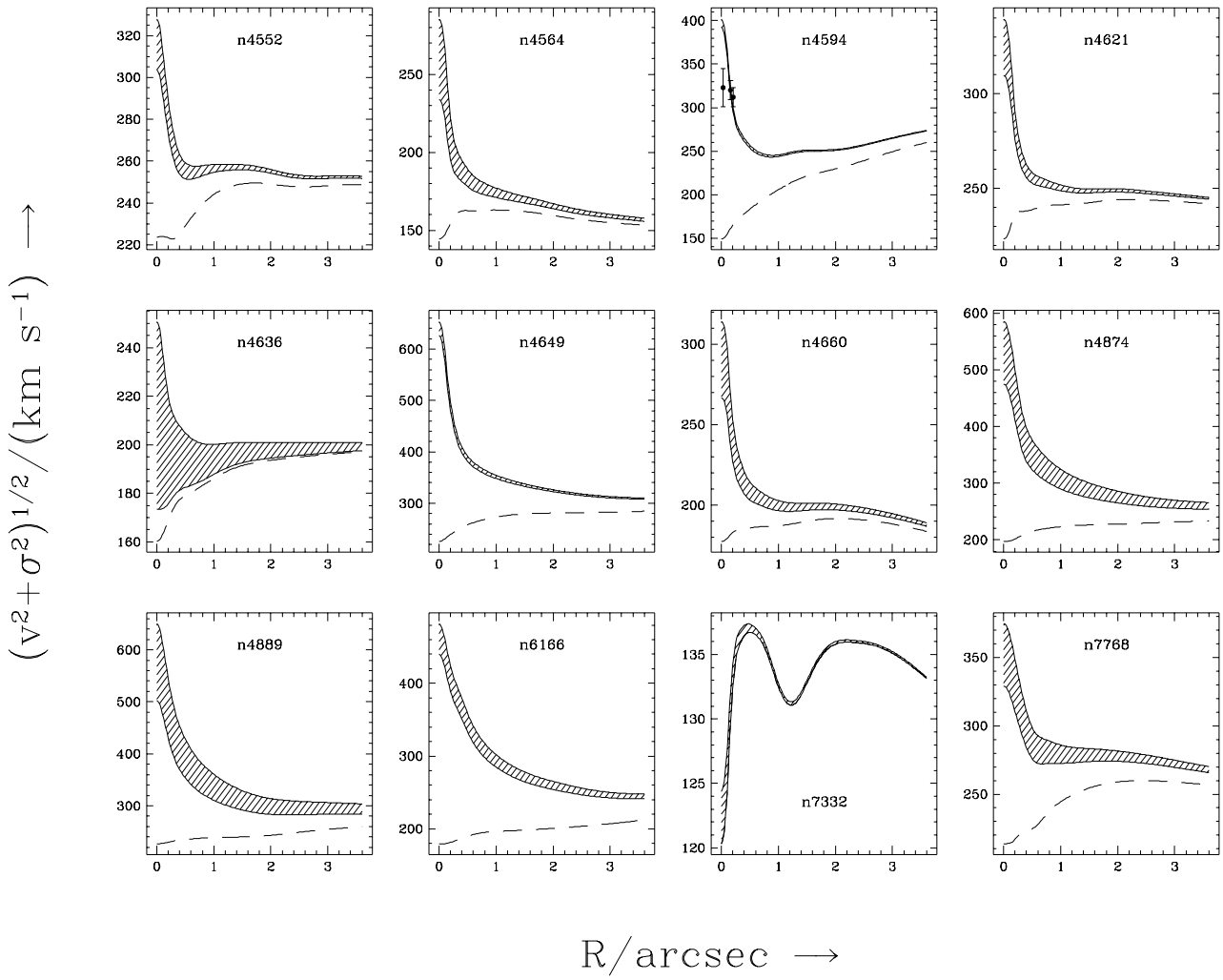

FIG. 7.—*Continued*

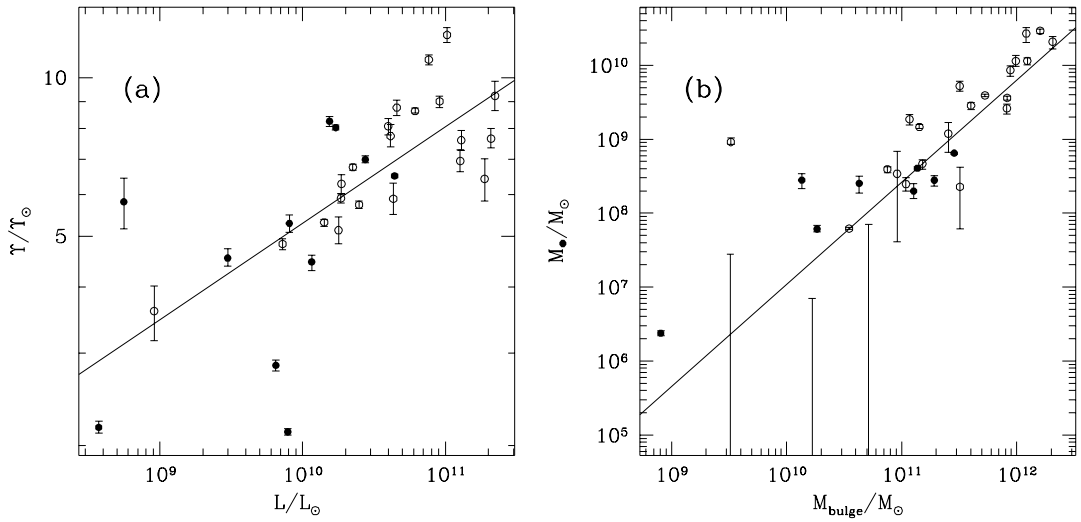

FIG. 8.—Correlations (*a*) between *V*-band stellar mass-to-light ratio Υ and bulge luminosity L and (*b*) between MDO mass $M_\bullet$ and M_{bulge} produced by our models. The filled and open circles plot power-law and core galaxies, respectively. The error bars give the 68% confidence intervals on Υ and $M_\bullet$. The solid lines plot Υ_{fit} and $M_{\bullet,fit}$ as described in the text (eqs. [10] and [11]).

TABLE 2

BEST-FITTING PARAMETERS FOR EACH GALAXY

Galaxy	D (Mpc)	$\log (L/L_\odot)$	$\log (\Upsilon_V/\Upsilon_{\odot,V})$	$\log (M_\bullet/M_\odot)$	$\log x$
M31	0.8	9.860	$0.684^{+0.010}_{-0.011}$	$7.792^{+0.016}_{-0.011}$	$-2.752^{+0.021}_{-0.017}$
M32	0.8	8.572	$0.335^{+0.012}_{-0.010}$	$6.376^{+0.035}_{-0.033}$	$-2.532^{+0.042}_{-0.043}$
NGC 821	19.5	10.188	$0.917^{+0.009}_{-0.010}$	$8.298^{+0.100}_{-0.103}$	$-2.807^{+0.107}_{-0.114}$
NGC 1399	17.9	10.616	$0.889^{+0.022}_{-0.021}$	$9.718^{+0.065}_{-0.068}$	$-1.785^{+0.075}_{-0.091}$
NGC 1600	50.2	11.012	$1.081^{+0.014}_{-0.014}$	$10.059^{+0.044}_{-0.056}$	$-2.046^{+0.064}_{-0.058}$
NGC 2300	31.8	10.660	$0.943^{+0.014}_{-0.015}$	$9.454^{+0.038}_{-0.054}$	$-2.155^{+0.055}_{-0.061}$
NGC 2778	33.6	10.064	$0.650^{+0.013}_{-0.016}$	<7.849	<-2.850
NGC 2832	90.2	11.112	$0.881^{+0.018}_{-0.019}$	$10.058^{+0.076}_{-0.072}$	$-1.935^{+0.089}_{-0.091}$
NGC 3115	8.4	10.232	$0.905^{+0.005}_{-0.005}$	$8.608^{+0.020}_{-0.024}$	$-2.530^{+0.024}_{-0.026}$
NGC 3377	9.9	9.812	$0.453^{+0.010}_{-0.011}$	$7.786^{+0.049}_{-0.041}$	$-2.469^{+0.045}_{-0.060}$
NGC 3379	9.9	10.152	$0.725^{+0.006}_{-0.008}$	$8.594^{+0.032}_{-0.048}$	$-2.287^{+0.042}_{-0.048}$
NGC 3608	20.3	10.268	$0.771^{+0.009}_{-0.008}$	$8.392^{+0.091}_{-0.091}$	$-2.638^{+0.088}_{-0.108}$
NGC 4168	36.4	10.636	$0.770^{+0.030}_{-0.030}$	$9.077^{+0.151}_{-0.253}$	$-2.356^{+0.194}_{-0.273}$
NGC 4278	17.5	10.396	$0.759^{+0.007}_{-0.007}$	$9.166^{+0.031}_{-0.021}$	$-1.983^{+0.030}_{-0.032}$
NGC 4291	28.6	10.272	$0.798^{+0.018}_{-0.019}$	$9.271^{+0.060}_{-0.079}$	$-1.807^{+0.081}_{-0.091}$
NGC 4467	15.3	8.748	$0.764^{+0.045}_{-0.051}$	<7.442	<-2.025
NGC 4472	15.3	10.960	$0.955^{+0.010}_{-0.011}$	$9.417^{+0.055}_{-0.074}$	$-2.509^{+0.074}_{-0.072}$
NGC 4473	15.8	10.252	$0.710^{+0.025}_{-0.026}$	$8.533^{+0.301}_{-0.923}$	$-2.456^{+0.329}_{-1.338}$
NGC 4486	15.3	10.884	$1.034^{+0.009}_{-0.010}$	$9.558^{+0.027}_{-0.029}$	$-2.357^{+0.031}_{-0.041}$
NGC 4486B	15.3	8.960	$0.557^{+0.048}_{-0.056}$	$8.963^{+0.055}_{-0.033}$	$-0.541^{+0.083}_{-0.100}$
NGC 4552	15.3	10.352	$0.830^{+0.005}_{-0.005}$	$8.668^{+0.051}_{-0.074}$	$-2.523^{+0.064}_{-0.071}$
NGC 4564	15.3	9.908	$0.723^{+0.017}_{-0.017}$	$8.404^{+0.097}_{-0.132}$	$-2.240^{+0.118}_{-0.136}$
NGC 4594	9.2	10.644	$0.813^{+0.003}_{-0.003}$	$8.811^{+0.005}_{-0.013}$	$-2.650^{+0.010}_{-0.013}$
NGC 4621	15.3	10.440	$0.844^{+0.007}_{-0.006}$	$8.445^{+0.061}_{-0.083}$	$-2.842^{+0.066}_{-0.086}$
NGC 4636	15.3	10.600	$0.908^{+0.014}_{-0.016}$	$8.356^{+0.267}_{-0.566}$	$-3.154^{+0.273}_{-0.652}$
NGC 4649	15.3	10.788	$0.937^{+0.006}_{-0.004}$	$9.592^{+0.016}_{-0.018}$	$-2.135^{+0.021}_{-0.020}$
NGC 4660	15.3	9.476	$0.657^{+0.017}_{-0.015}$	$8.446^{+0.090}_{-0.115}$	$-1.699^{+0.110}_{-0.120}$
NGC 4874	93.3	11.348	$0.966^{+0.028}_{-0.028}$	$10.319^{+0.071}_{-0.097}$	$-2.000^{+0.093}_{-0.119}$
NGC 4889	93.3	11.276	$0.808^{+0.038}_{-0.042}$	$10.429^{+0.079}_{-0.119}$	$-1.678^{+0.127}_{-0.140}$
NGC 6166	112.5	11.320	$0.884^{+0.020}_{-0.018}$	$10.467^{+0.025}_{-0.035}$	$-1.745^{+0.045}_{-0.047}$
NGC 7332	20.3	9.896	$0.327^{+0.006}_{-0.006}$	<6.845	<-3.373
NGC 7768	103.1	11.104	$0.842^{+0.021}_{-0.020}$	$9.933^{+0.060}_{-0.081}$	$-2.027^{+0.089}_{-0.091}$

NOTES.—The best-fitting parameters (Υ_V, $M_\bullet$, and $x \equiv M_\bullet/M_{\rm bulge}$) with their 68% confidence intervals for the 32 galaxies that our models describe well. The assumed galaxy distance D and the luminosity L of the bulge or other hot stellar component are also listed.

where we have defined

$$\Pr(D \mid x) \equiv \int \Pr(D \mid \Upsilon x)\, \Pr(\Upsilon) d\Upsilon\,, \qquad (16)$$

and similarly for $\Pr(D_j \mid x_j)$.

The posterior distributions $\Pr(\omega \mid D, P)$ for each parameterization are plotted in Figure 10. Table 4 lists the best-fitting parameters with their 68% confidence intervals, and Figure 11*a* plots $\Pr(x \mid \omega, P)$ for the best-fitting parameters ω in each case. According to all parameterizations except $P_{\rm PL1}$, nearly all galaxies have MDOs ($f \simeq 0.96$) with means $\langle x \rangle \simeq 0.01$ and $\langle \log x \rangle \simeq -2.25$, consistent with the KR95 interpretation. However, the best-fitting parameters from

TABLE 3

THE FIVE PARAMETERIZATIONS FOR $\Pr(x \mid \omega)$

P	ω	$\Pr_+(x \mid \omega)$
Power law 1: $P_{\rm PL1}$	$(f, \log x_0, \alpha)$	Nx^α if $x < x_0$, zero otherwise ($\alpha > -1$)
Power law 2: $P_{\rm PL2}$	$(f, \log x_0, \alpha)$	Nx^α if $x > x_0$, zero otherwise ($\alpha < -1$)
Schechter: $P_{\rm S}$	$(f, \log x_0, \alpha)$	$N(x/x_0)^\alpha \exp(-x/x_0)$ ($\alpha > -1$)
Gaussian: $P_{\rm G}$	$(f, \log x_0, \log \Delta)$	$N \exp[-\frac{1}{2}(x - x_0)^2/\Delta^2]$
Log Gaussian: $P_{\rm LG}$	$(f, \log x_0, \log \Delta)$	$N \exp[-\frac{1}{2}(\log x - \log x_0)^2/\Delta^2](1/x)$

NOTES.—The variable $x \equiv M_\bullet/M_{\rm bulge}$, where $M_\bullet$ is the mass of the MDO and $M_{\rm bulge}$ is the mass of the hot stellar component of the galaxy. For a given set of parameters ω, the probability that a galaxy has an MDO with mass in the range $[x, x + dx]$ is $\Pr(x \mid \omega, P)dx = (1 - f)\delta(x)dx + f \Pr_+(x \mid \omega, P)dx$, where f is the fraction of galaxies with $M_\bullet > 0$ and the $N(\omega)$ in $\Pr_+(x \mid \omega, P)$ is a normalizing factor (eq. [12]). The prior probability $\Pr(\omega \mid P)$ is assumed to be flat in the parameters ω.

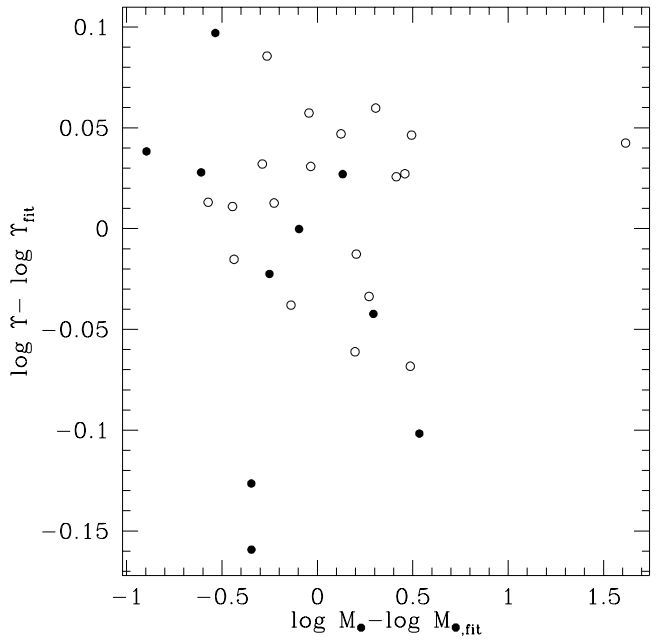

FIG. 9.—Correlation of the residuals in the Υ vs. L and M_a vs. $M_{\rm bulge}$ fits. As in Fig. 8, the open and closed circles are used to distinguish between core and power-law galaxies.

both $P_{\rm PL2}$ and $P_{\rm LG}$ imply that there is a genuine ridge in Pr (x) at this mean x, whereas both $P_{\rm PL1}$ and $P_{\rm S}$ say there is *no* ridge, since they prefer $\alpha < 0$. The Gaussian parameterization $P_{\rm G}$ is inconclusive: there is not a strong lower limit on x_0 in this case, since the most likely value of the other parameter Δ is comparable in size to x_0.

Which of the five parameterizations yield the better description of the real Pr (x)? Using Bayes's theorem again, the plausibility of the parameterization P given the available data D is

$$\Pr(P\,|\,D) = \frac{\Pr(P)\,\Pr(D\,|\,P)}{\Pr(D)} = \frac{\Pr(P)}{\Pr(D)}\int \Pr(D\,|\,\omega, P)\,\Pr(\omega\,|\,P)d\omega\,. \quad (17)$$

If we assume that all of the parameterizations are a priori equally likely, i.e., Pr $(P_{\rm PL1})$ = Pr $(P_{\rm PL2})$ = Pr $(P_{\rm S})$ = Pr $(P_{\rm G})$ = Pr $(P_{\rm LG})$, then we find that Pr $(P_{\rm PL2}\,|\,D) = 4$ Pr $(P_{\rm LG}\,|\,D) \simeq 2 \times 10^5$ Pr $(P_{\rm S}\,|\,D) \simeq 10^{10}$ Pr $(P_{\rm PL1}\,|\,D) \simeq 10^{12}$ × Pr $(P_{\rm G}\,|\,D)$: $P_{\rm PL2}$ and $P_{\rm LG}$ provide by far the best description of the five. This result suggests that there really is a ridge in Pr (x) at $\log x \simeq -2.2$.

It is also instructive to try to obtain a "nonparametric" estimate of Pr (x). We take n parameters $\omega_1, \ldots, \omega_n$, with $n = 50$. We define ω_i as the probability that a randomly chosen galaxy has an MDO whose mass lies between x_{i-1} and x_i, where the x_i run logarithmically from $x_1 = 10^{-5}$ to $x_{50} = 1$ and $x_0 = 0$. A reasonable prior guess for Pr (x) (and therefore the ω_i) is a power law. So we choose

$$\log \Pr(\omega) = -\frac{\lambda}{n}\sum_{i=2}^{n-1}\left(\frac{\log \omega_{i+1} - 2\log \omega_i + \log \omega_{i-1}}{\Delta \log x}\right)^2, \quad (18)$$

where the free parameter λ controls how smooth (i.e., how far from a pure power law) we think an acceptable Pr (x) ought to be. We use 10^6 iterations of the Metropolis algorithm (Metropolis et al. 1953; see also Saha & Williams 1994) to obtain the posterior distribution Pr $(\omega\,|\,D)$ for each ω_i for a range of λ. The results for $\lambda = 5$ are plotted in Figure 11*b*. The "nonparametric" distributions Pr (x) calculated in this way are bimodal, but are otherwise broadly the same as those obtained from the best parameterizations $P_{\rm PL2}$ and $P_{\rm LG}$. The lower mode (at $x \simeq -2.5$) corresponds to power-law galaxies, and the upper (at $x \simeq -1.9$) to core galaxies.

Thus far we have assumed that the MDO mass distribution depends only on $x \equiv M_\bullet/M_{\rm bulge}$, but there is no good reason for assuming that $M_\bullet$ should be correlated with the mass rather than, say, the luminosity of the bulge. Consider a more general form,

$$x' \equiv \left(\frac{M_\bullet}{1\ M_\odot}\right)\left(\frac{1\ L_\odot}{L}\right)\left(\frac{1\ \Upsilon_\odot}{\Upsilon}\right)^a, \quad (19)$$

where a is a free parameter. The analysis above can be carried out with x replaced by x'. Setting $a = 1$ tests the correlation of $M_\bullet$ with $M_{\rm bulge}$ (the case we have just considered), whereas setting $a = 0$ tests its correlation with L. The results of our calculations of Pr $(D\,|\,P, a)$ for a range of a are plotted in Figure 12. Clearly, the case $a = 1$ is the most plausible—$M_\bullet$ is more strongly correlated with the mass of the bulge than with the luminosity. For the $P_{\rm PL2}$ parameterization the 68% confidence interval on a is $a = 1.0 \pm 0.4$, while $a = 1.0 \pm 0.6$ for $P_{\rm LG}$.

Given the hints in Figures 8*b* and 11*b* that the masses of the MDOs in core galaxies may be distributed differently from those in power-law galaxies, it is worth repeating the analysis above for each type of galaxy separately. We find that the power-law and core galaxies do indeed have different best-fit distributions. For example, Figure 13 plots the probability distributions Pr $(D_\cap\,|\,P_{\rm PL2}, a)$ and Pr $(D_\setminus\,|\,P_{\rm PL2},$

TABLE 4

BEST-FITTING PARAMETERIZED PROBABILITY DISTRIBUTIONS

P	f	$\log x_0$	α or $\log \Delta$	$\log \langle x\rangle$	$\langle \log x\rangle$
$P_{\rm PL1}$	$1.000^{+0.000}_{-0.057}$	$-0.633^{+0.125}_{-0.100}$	$-0.784^{+0.056}_{-0.037}$	$-1.347^{+0.115}_{-0.111}$	$-3.178^{+0.893}_{-0.893}$
$P_{\rm PL2}$	$0.950^{+0.032}_{-0.062}$	$-2.790^{+0.031}_{-0.063}$	$-1.725^{+0.131}_{-0.173}$		$-2.268^{+0.097}_{-0.087}$
$P_{\rm S}$	$1.000^{+0.000}_{-0.067}$	$-1.705^{+0.204}_{-0.109}$	$-0.456^{+0.178}_{-0.122}$	$-1.880^{+0.117}_{-0.108}$	$-2.338^{+0.153}_{-0.188}$
$P_{\rm G}$	$0.940^{+0.042}_{-0.067}$	$-2.930^{+0.325}_{-0.000}$	$-1.717^{+0.098}_{-0.082}$	$-1.808^{+0.105}_{-0.096}$	$-1.992^{+0.106}_{-0.091}$
$P_{\rm LG}$	$0.970^{+0.030}_{-0.055}$	$-2.281^{+0.100}_{-0.100}$	$-0.289^{+0.060}_{-0.065}$	$-1.965^{+0.143}_{-0.119}$	$-2.282^{+0.103}_{-0.109}$

NOTES.—The best-fitting parameters ω and their 68% confidence limits for each assumed distribution Pr $(x\,|\,\omega, P)$. By definition, $0 \le f \le 1$. The last two columns give the logarithm of the expectation value of $x \equiv M_\bullet/M_{\rm bulge}$ and the expectation value of $\log x$ for those galaxies with $M_\bullet \neq 0$ [both calculated from $\Pr_+(x\,|\,\omega, P)$]. The mean $\langle x\rangle$ does not exist for $P_{\rm PL2}$.

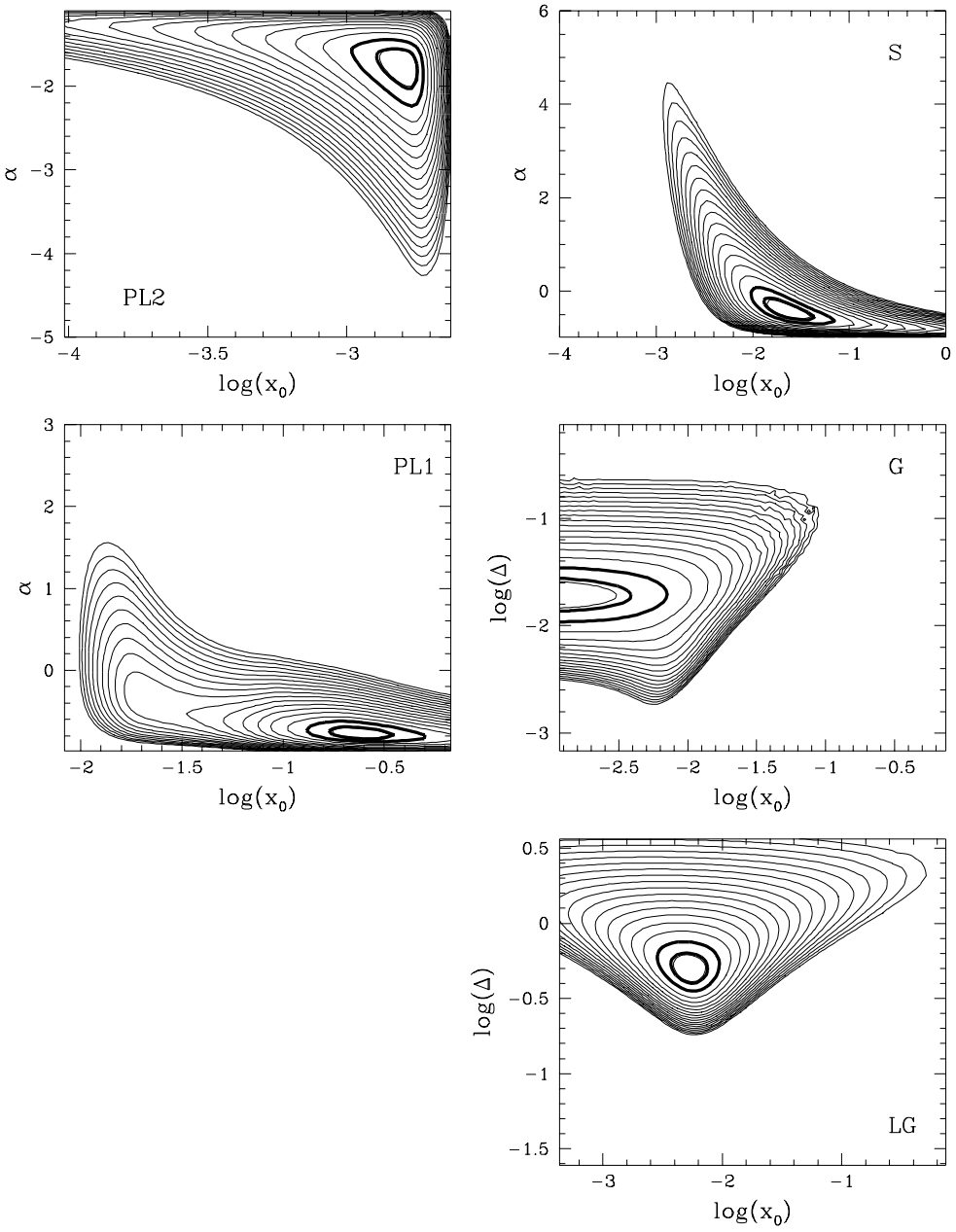

FIG. 10.—Posterior distributions Pr ($\omega \mid D$, P) marginalized over f for $P_{\rm PL1}$, $P_{\rm PL2}$, $P_{\rm S}$, $P_{\rm G}$, and $P_{\rm LG}$. Successive light contours correspond to a factor of 10 change in Pr ($\omega \mid D$, P). The heavy contours enclose the 68% and 95% confidence areas of the parameters ω. The most likely value of f within the 95% confidence area in all five cases is ~ 0.97.

a) for core and power-law galaxies, respectively. For core galaxies $a = 1.6^{+0.1}_{-0.2}$ and $\langle \log x' \rangle \simeq -2.1 \pm 0.6$, while for power laws $a = 0.6^{+0.2}_{-0.3}$ and $\langle \log x' \rangle \simeq -2.0 \pm 0.3$. We obtain similar results for the $P_{\rm LG}$ parameterization.

By how much does treating core and power-law galaxies separately improve the description of the $M_\bullet$ distribution? Let H_1 be the hypothesis that the x' distribution is the same for all galaxies, and H_2 be the alternative hypothesis that power-law and core galaxies have separate, distinct distributions. Proceeding analogously to equation (17), we have that

$$\Pr(H_1 \mid D, P) = \frac{\Pr(H_1)}{\Pr(D, P)} \Pr(D, P \mid H_1) = \frac{\Pr(H_1)}{\Pr(D)\Pr(P)} \int \Pr(D \mid a, P) \Pr(a) da \, . \quad (20)$$

Similarly,

$$\Pr(H_2 \mid D, P) = \frac{\Pr(H_2)}{\Pr(D)\Pr(P)} \left[\int \Pr(D_\cap \mid a, P) \Pr(a) da \right] \times \left[\int \Pr(D_\setminus \mid a, P) \Pr(a) da \right] . \quad (21)$$

Taking Pr (H_1) = Pr (H_2) and Pr (a) uniform in a, we find for the best parameterization $P_{\rm PL2}$ that Pr ($H_2 \mid D$, $P_{\rm PL2}$)/Pr ($H_1 \mid D$, $P_{\rm PL2}$) $\simeq 15$. Thus, treating the two types of galaxies as separate populations is *formally* about "two sigma" better than treating them identically. This result is, of course, contingent on the validity of our relatively crude two-integral models and, therefore, cannot be considered very robust.

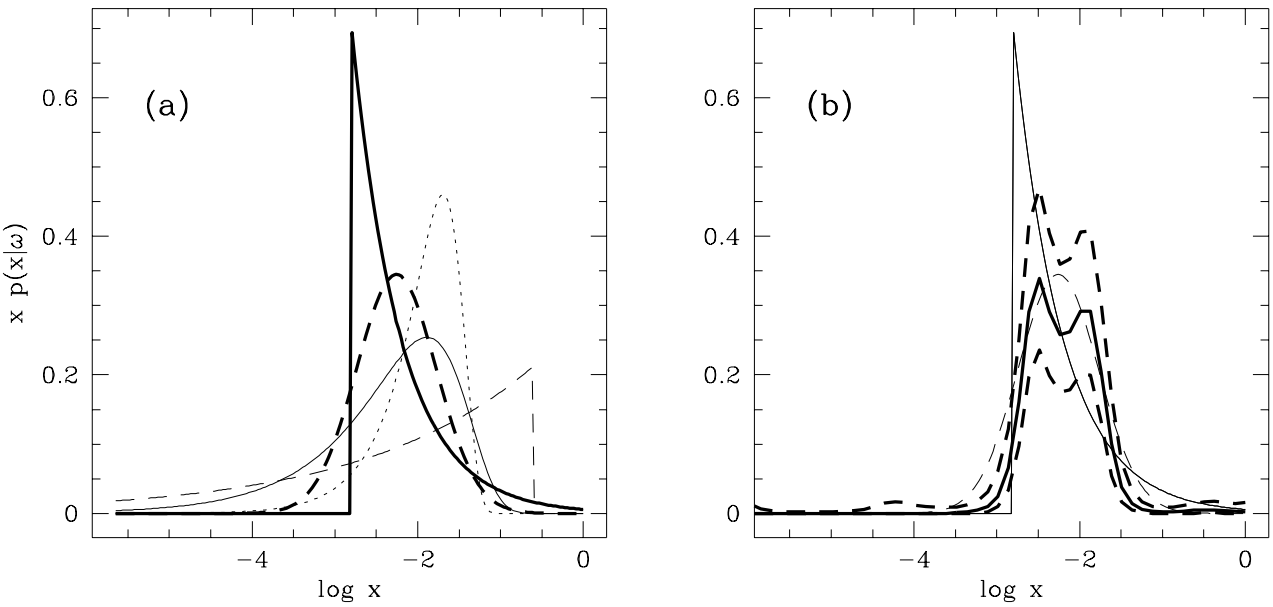

FIG. 11.—(*a*) Probability distributions Pr $(x \mid \omega, P)$ for the best-fitting parameters ω. The heavy solid and dashed curves show results for P_{PL2} and P_{LG}, the two best-fitting cases. The light solid, dashed, and dotted curves are for P_S, P_{PL1}, and P_G, respectively. (*b*) "Nonparametric" probability distribution Pr (x) (*heavy solid curve*) and its 68% confidence limits (*heavy dashed curves*) obtained using the Metropolis algorithm with $\lambda = 5$. The best-fitting parameterized distributions P_{PL2} and P_{LG} are overlaid as the light solid and dashed curves, respectively.

6. CONCLUSIONS

We have examined a sample of 36 galaxy bulges and found that the kinematics of 32 of them are described well by two-integral axisymmetric models. Among these 32, a substantial MDO is required in all but four in order for our models to reproduce the observed kinematics. We have considered a range of models for the demography of these MDOs. In the best-fitting models, about 97% of galaxies have an MDO. The mass of this MDO is correlated with the bulge mass, with an MDO-to-bulge mass ratio of around 0.005, although there are hints of differences between core and power-law galaxies. Possible explanations for this correlation have already been discussed by Faber et al. (1997). The galaxies without MDOs perhaps have a different formation history; one possible scenario has been put forward by Kormendy (1993b).

The mass-to-light ratios Υ fitted by our models scale with luminosity L as $\Upsilon \propto L^{0.2}$, which is just the usual fundamental-plane correlation. Since our models take full account of the shape of the light distribution of each galaxy,

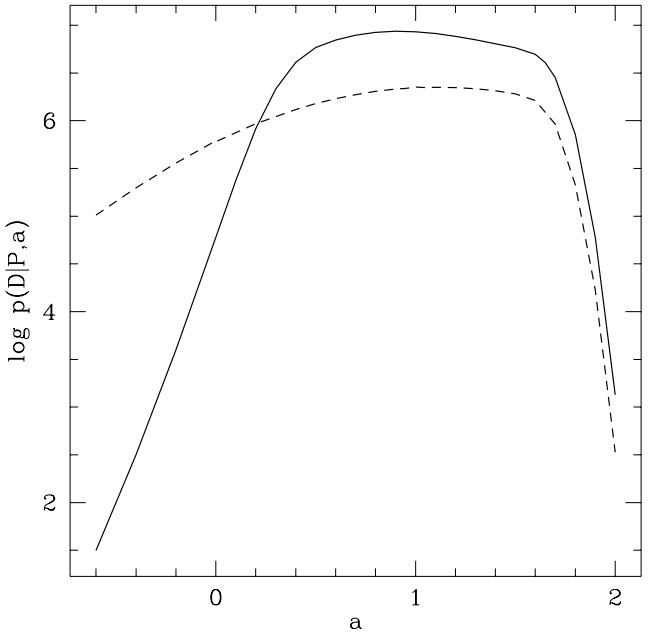

FIG. 12.—Variation of Pr $(D \mid P,a)$ with a, where a is defined in eq. (19). The solid and dashed curves show $P = P_{PL2}$ and $P = P_{LG}$, respectively. The vertical scale does not extend down far enough to show the results for the other three parameterizations.

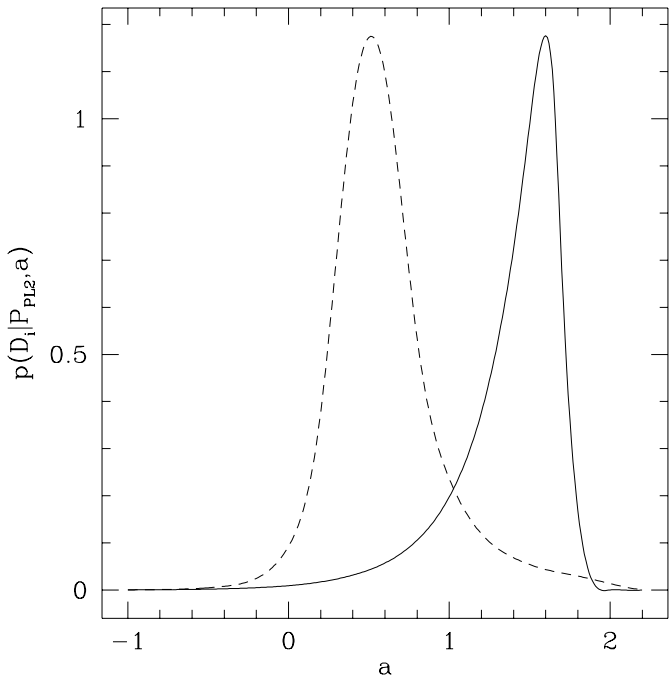

FIG. 13.—Likelihood distributions Pr $(D_\cap \mid P_{PL2}, a)$ (*solid curve*) for core and Pr $(D_\setminus \mid P_{PL2}, a)$ (*dashed curve*) for power-law galaxies.

they rule out any attempts to explain the slope of the fundamental plane by a "nonhomology" of the light profiles (e.g., Graham & Colless 1997 and references therein). Our models do not, however, consider the possibility of a systematic change in orbital anisotropy with luminosity (Ciotti, Lanzoni, & Renzini 1996).

These results are based on an "assembly line" approach to building galaxy models, which is necessarily less accurate than building models for each galaxy by hand. In particular:

1. Some or all of the galaxies may not be axisymmetric.
2. Even if the galaxies are axisymmetric, our two-integral models are not the most general possible. For some or all of the galaxies, there may exist more general three-integral models that can reproduce the observed kinematics (and, indeed, the full line-of-sight velocity profiles) without needing to invoke MDOs—see Kormendy et al. (1997) and Appendix B for examples.
3. The selection criteria used to derive this sample are heterogeneous and impossible to quantify, although any biases introduced by properties such as luminosity, core size, and surface brightness are accounted for by the analysis procedure in § 3.
4. The assumption that the mass-to-light ratio is independent of position outside the center may not be correct.

Of the points above, the most important is perhaps (2)—our conclusions are most uncertain because of our assumption of a two-integral distribution function. We should know soon whether more general three-integral models (e.g., Rix et al. 1997; Gebhardt et al. 1997; Richstone et al. 1998) will relax the need for MDOs in at least some of the galaxies in our sample.

We thank Jesús González for providing kinematic data from his thesis, Barbara Ryden, Roeland van der Marel, and the anonymous referee for constructive criticism of the material in this paper, and L. Danese for pointing out an error in an early version of this paper. Our collaboration was supported by *HST* data analysis funds through GO grants GO-2600.01-87A and GO-06099.01-94A, by NASA grant NAS 5-1661 to the WF/PC-1 Instrument Definition Team, and by grants from NSERC. S. T. acknowledges support from an Imasco fellowship. We thank the Fields Institute for Research in Mathematical Sciences at the University of Toronto and the Observatories of the Carnegie Institution of Washington for their hospitality during part of this work.

APPENDIX A

NOTES ON INDIVIDUAL GALAXIES

M31.—This galaxy has a double nucleus (see, e.g., Lauer et al. 1993), but axisymmetric models should still provide a reasonable description of the gross features of its kinematics. We use kinematic data from van der Marel et al. (1994) and Kormendy & Bender (1998). The former appear to measure major-axis radii from the photometric center of the galaxy, rather than the kinematic center, which we assume to be coincident with the fainter nucleus (e.g., Tremaine 1995). Thus we add 0.″3 to van der Marel et al.'s quoted major-axis positions. We do not fit to kinematic data beyond 10″, because the outer photometry we use (Kent 1987) consists only of a major- and a minor-axis profile with no additional isophote-shape information.

NGC 1600.—Both Jedrzejewski & Schechter (1989) and Bender, Saglia, & Gerhard (1994) give major- and minor-axis kinematics for this galaxy. There are many more outlier points in the latter data, so we reject it.

NGC 2778.—Fisher, Illingworth, & Franx (1995) and González (1993) give major-axis profiles. Both González and Jedrzejewski & Schechter (1989) give minor-axis profiles. Fisher et al.'s central dispersion is inconsistent with the others, so we reject their data for this galaxy.

NGC 3379.—The best kinematic data come from Gebhardt et al. (1997). We restrict our model fits to their ground-based data within 12″ of the center.

NGC 4486.—We use the blue G-band kinematics from van der Marel (1994) and reject his infrared kinematics, which are probably affected by template mismatch. In the same paper, van der Marel presents evidence that this galaxy is radially anisotropic in its outer parts. Therefore we restrict our model fits to the kinematics within the innermost 5″.

NGC 4594.—The ground-based outer photometry (Kormendy 1988) consists only of a major- and a minor-axis profile. Because of this, and because of the problems with dust obscuration, we only use kinematic data within 8″.

APPENDIX B

TWO-INTEGRAL VERSUS RADIALLY ANISOTROPIC MODELS

There have been a couple of claims that two-integral models cannot describe the dynamics of certain types of real galaxies (van der Marel 1991; Bender et al. 1994, hereafter BSG). While we would find it remarkable if all the galaxies in our sample were close to two-integral models, we nevertheless consider it worthwhile to show here that these claims do not stand up to close scrutiny. For balance, we then consider the possibility that some of our galaxies may be radially anisotropic.

BSG compared the line-of-sight velocity profiles (VPs) of real galaxies with those predicted by two-integral models. It is convenient to parameterize VP shapes using the van der Marel & Franx (1993) Gauss-Hermite series, which gives the best-fit Gaussian to each VP along with coefficients $h_3, h_4, \ldots$, that describe the deviations of the VP from Gaussian. VPs with $h_4 > 0$ are more "triangular" than Gaussian, while those with $h_4 < 0$ are more "square." BSG note that nonrotating flattened core galaxies with boxy isophote distortions generally have major-axis VPs that are fairly close to Gaussian ($h_4 \simeq 0$), whereas two-integral models predict major-axis VPs with $h_4 < 0$ (i.e., the model VPs are more "square"). This discrepancy would appear to rule out two-integral models for this class of galaxies.

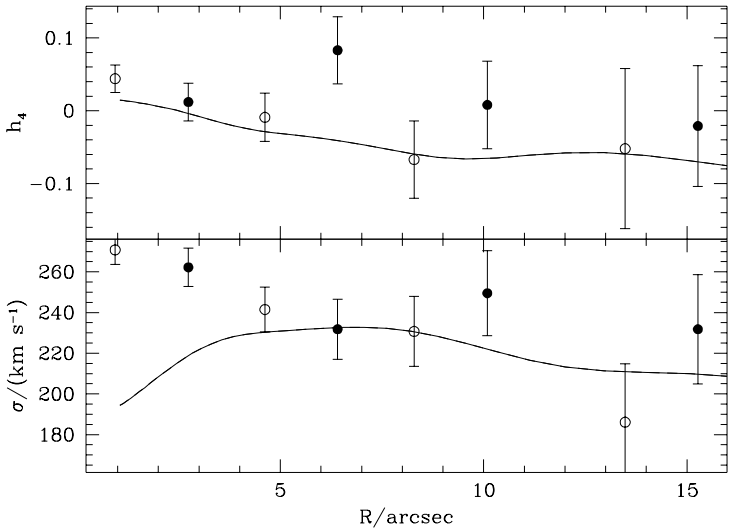

FIG. 14.—Gauss-Hermite coefficients of the major-axis VPs of a two-integral model of the nonrotating boxy elliptical NGC 2300 without an MDO (*curves*). These predictions agree quite well with the observed VPs (*circles*) outside about 5″.

There are two such galaxies (NGC 1600 and NGC 2300) in our sample whose VPs have been measured, in both cases by BSG. We have used Magorrian & Binney's (1994) method to construct two-integral models for each. Figure 14 shows the Gauss-Hermite coefficients of the VPs predicted in this way for a model of NGC 2300 without an MDO. Unfortunately, Magorrian & Binney's moment-based method is unable to predict the VPs of models with MDOs, but the predictions of this MDO-less model agree quite well with the observations outside the MDO's sphere of influence (about 5″). We find similar results for NGC 1600 and conclude that the VPs are consistent with two-integral models, at least for these galaxies.

A second objection to two-integral models has been made by van der Marel (1991). Using (the square root of) the observed major- and minor-axis projected second moments $\mu_{j,\mathrm{maj}}(R_i)$ and $\mu_{j,\mathrm{min}}(R_i)$ and the corresponding predictions $\hat{\mu}_{j,\mathrm{maj}}(R_i)$ and $\hat{\mu}_{j,\mathrm{min}}(R_i)$ from two-integral models, he calculated the quantity

$$\bar{\mathscr{R}} \equiv \sum_i \frac{\mu_{j,\mathrm{maj}}(R_i)}{\mu_{j,\mathrm{min}}(R_i)} \Big/ \sum_i \frac{\hat{\mu}_{j,\mathrm{maj}}(R_i)}{\hat{\mu}_{j,\mathrm{min}}(R_i)} \tag{B1}$$

for each of a sample of galaxies. One would expect $\bar{\mathscr{R}} = 1$ if a galaxy were two-integral, but van der Marel found a wide scatter in $\bar{\mathscr{R}}$ in his sample, with a slight bias toward $\bar{\mathscr{R}} > 1$. This result suggests that two-integral models predict too much motion on the major axis relative to the minor.

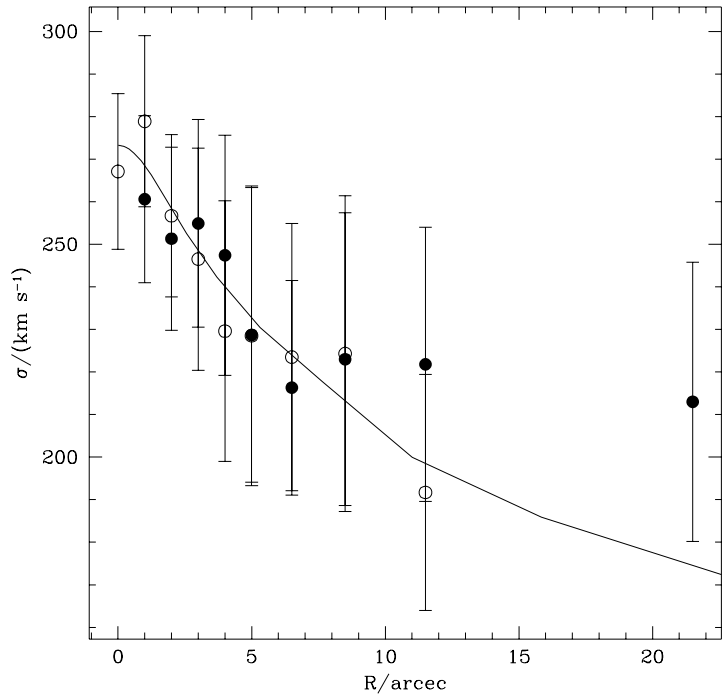

FIG. 15.—Projected velocity dispersion profile of an anisotropic ($\beta = 0.4$) spherical model of NGC 2300 without an MDO (*curve*). The circles plot the observed dispersion profile.

The problem with this analysis is that the "observed" second moments μ were obtained from the observed rotational velocities V and velocity dispersions σ assuming that V and σ measure the classical first- and second-order moments of the underlying VP and thus that $\mu^2 = V^2 + \sigma^2$. However, as van der Marel & Franx (1993) point out, the V and σ yielded by observations measure the mean and dispersion of the *best-fit Gaussian* to the VP and have no simple direct relation to the VP's classical moments predicted by models (see also Fig. 1). For example, taking the V's and σ's of the best-fit Gaussians to the VPs of our two-integral model of NGC 2300 as "observations" and comparing with the classical moments, we find $\bar{\mathcal{R}} = 1.08$, comparable to the largest values of $\bar{\mathcal{R}}$ reported by van der Marel. Thus, an observer repeating van der Marel's analysis in an imaginary universe of two-integral galaxies would find that $\bar{\mathcal{R}} \neq 1$ and erroneously rule out two-integral models.

While we believe that no one has conclusively ruled out two-integral models as descriptions of real nontriaxial galaxies, there is no compelling reason to believe that nature favors such models either. For example, it is possible that the observed central rise in the second-moment profiles of many of our galaxies (§ 4) could be due to a bias toward radial orbits rather than an MDO. To test this possibility, we have constructed a range of radially anisotropic spherical models with constant mass-to-light ratio for each of the 15 roundest galaxies in our sample. These models have constant anisotropy $\beta \equiv 1 - \sigma_\theta^2/\sigma_r^2$, where σ_θ and σ_r are the tangential and radial velocity dispersions. It is straightforward to calculate the projected velocity dispersion profile of such models using the Jeans equations (e.g., Binney & Tremaine 1987, § 4). For each of the 15 galaxies we find that a model without an MDO and a constant radial anisotropy somewhere between $\beta \simeq 0.3$ and $\beta \simeq 0.7$ provides just as good a fit to the observed kinematics as does an isotropic ($\beta = 0$) model with an MDO. For example, Figure 15 shows the predictions for an anisotropic model of NGC 2300 with $\beta = 0.4$ and no MDO.

The simplest distribution functions for these constant-anisotropy models are of the form $f(E, L^2) = L^{-2\beta} f_0(E)$, where E and L are the binding energy and angular momentum and the function $f_0(E)$ depends on the density profile $\nu(r)$ and potential $\Phi(r)$. A numerical method to find $f_0(E)$ given $\nu(r)$ and $\Phi(r)$ will be described in a forthcoming paper. Using this method, we find that for most of these anisotropic models $f_0(E)$ is required to be negative in places, meaning that the models are unphysical. On the other hand, this problem does not arise for our isotropic models with MDOs: we find that they have sensible nonnegative distribution functions.

REFERENCES

Bender, R., Burstein, D., & Faber, S. M. 1992, ApJ, 399, 462
Bender, R., Döbereiner, S., & Möllenhoff, C. 1987, A&A, 177, 53
Bender, R., Kormendy, J., & Dehnen, W. 1996, ApJ, 464, L119
Bender, R., & Nieto, J.-L. 1990, A&A, 239, 97
Bender, R., Saglia, R. P., & Gerhard, O. E. 1994, MNRAS, 269, 785 (BSG)
Binney, J. J., Davies, R. L., & Illingworth, G. D. 1990, ApJ, 361, 78
Binney, J. J., & Tremaine, S. 1987, Galactic Dynamics (Princeton: Princeton University Press)
Byun, Y.-I., et al. 1996, AJ, 111, 1889
Ciotti, L., Lanzoni, B., & Renzini, A. 1996, MNRAS, 282, 1
Davies, R. L., & Birkinshaw, M. 1988, ApJS, 68, 409
Dehnen, W. 1993, MNRAS, 265, 250
Dehnen, W., & Gerhard, O. E. 1994, MNRAS, 268, 1019
Dejonghe, H. 1986, Phys. Rep., 133, 218
Faber, S. M., Dressler, A., Davies, R. L., Burstein, D., Lynden-Bell, D., Terlevich, R., & Wegner, G. 1987, in Nearly Normal Galaxies, ed. S. M. Faber (New York: Springer), 317
Faber, S. M., et al. 1997, AJ, 114, 1771
Fisher, D., Illingworth, G., & Franx, M. 1994, AJ, 107, 160
———. 1995, ApJ, 438, 539
Forbes, D. A., Franx, M., & Illingworth, G. D. 1995, AJ, 109, 1988
Forbes, D. A., Franx, M., Illingworth, G. D., & Carollo, C. M. 1996, ApJ, 467, 126
Franx, M., Illingworth, G., & Heckman, T. 1989, ApJ, 344, 613
Gebhardt, K., et al. 1996, AJ, 112 105
———. 1997, AJ, submitted
González, J. 1993, Ph.D. thesis, Univ. California Santa Cruz
Graham, A., & Colless, M. 1997, MNRAS, 287, 221
Grillmair, C. J., Faber, S. M., Lauer, T. R., Baum, W. A., Lynds, C. R., O'Neil, E. J., Jr., & Shaya, E. J. 1994, AJ, 108, 102
Harms, R. J., et al. 1994, ApJ, 435, L35
Jaffe, W. 1983, MNRAS, 202, 995
Jaffe, W., Ford, H. C., O'Connell, R. W., van den Bosch, F. C., & Ferrarese, L. 1994, AJ, 108, 1567
Jedrzejewski, R., & Schechter, P. L. 1989, AJ, 98, 147
Kent, S. M. 1987, AJ, 94, 306
Kormendy, J. 1988, ApJ, 335, 40
———. 1993a, in The Nearest Active Galaxies, ed. J. E. Beckman, L. Colina, & H. Netzer (Madrid: CSIC), 197
———. 1993b, in IAU Symp. 153, Galactic Bulges, ed. H. Dejonghe & H. J. Habing (Dordrecht: Kluwer), 209
Kormendy, J., & Bender, R. 1998, in preparation
Kormendy, J., et al. 1996a, ApJ, 473, L91
Kormendy, J., Bender, R., Evans, A. S., & Richstone, D. 1998, AJ, 115, 1823
Kormendy, J., et al. 1997, ApJ, 482, L139
———. 1996b, ApJ, 459, L57
Kormendy, J., & Richstone, D. 1992, ApJ, 393, 559
———. 1995, ARA&A, 33, 581 (KR95)
Lauer, T. R., et al. 1995, AJ, 110, 2622
———. 1992a, AJ, 104, 552
———. 1993, AJ, 106, 1436
———. 1992b, AJ, 103, 703
Lynden-Bell, D. 1962, MNRAS, 123, 447
Magorrian, J. 1998, MNRAS, in press
Magorrian, J., & Binney, J. 1994, MNRAS, 271, 949
Metropolis, N., Rosenbluth, A. W., Rosenbluth, M. N., Teller, A. H., & Teller, E. 1953, J. Chem. Phys., 21, 1087
Peletier, R. F., Davies, R. L., Illingworth, G. D., Davis, L. E., & Cawson, M. 1990, AJ, 100, 1091
Richstone, D., Bower, G., & Dressler, A. 1990, ApJ, 353, 118
Richstone, D., et al. 1998, in preparation
Rix, H.-W., de Zeeuw, P. T., Cretton, N., van der Marel, R. P., & Carollo, C. M. 1997, ApJ, 488, 702
Romanowsky, A. J., & Kochanek, C. S. 1997, MNRAS, 287, 35
Rybicki, G. 1987, in IAU Symp. 127, Structure and Dynamics of Elliptical Galaxies, ed. P. T. de Zeeuw (Dordrecht: Reidel), 397
Saha, P., & Williams, T. B. 1994, AJ, 107, 1295
Sargent, W. L. W., Young, P. J., Lynds, C. R., Boksenberg, A., Shortridge, K., & Hartwick, F. D. A. 1978, ApJ, 221, 731
Scorza, C., & Bender, R. 1995, AJ, 293, 20
Tremaine, S. 1995, AJ, 110, 628
Tremaine, S., Richstone, D. O., Byun, Y.-I., Dressler, A., Faber, S. M., Grillmair, C., Kormendy, J., & Lauer, T. R. 1994, AJ, 107, 634
Tremblay, B., & Merritt, D. 1995, AJ, 110, 1039
van der Marel, R. P. 1991, MNRAS, 253, 710
———. 1994, MNRAS, 270, 271
van der Marel, R. P., de Zeeuw, P. T., & Rix, H.-W. 1997a, ApJ, 488, 119
van der Marel, R. P., de Zeeuw, P. T., Rix, H.-W., & Quinlan, G. D. 1997b, Nature, 385, 610
van der Marel, R. P., & Franx, M. 1993, ApJ, 407, 525
van der Marel, R. P., Rix, H.-W., Carter, D., Franx, M., White, S. D. M., & de Zeeuw, T. 1994, MNRAS, 268, 521